

Hafnium(IV) Chemistry with Imide–Dioxime and Catecholate–Oxime Ligands: Unique $\{Hf_5\}$ and Metalloaromatic $\{Hf_6\}$ –Oxo Clusters Exhibiting Fluorescence

Stamatis S. Passadis, Sofia Hadjithoma, Nicola J. Fairbairn, Gordon J. Hedley, Nuno A. G. Bandeira,* Athanassios C. Tsipis,* Haralampos N. Miras,* Anastasios D. Keramidas,* and Themistoklis A. Kabanos*



Cite This: *Inorg. Chem.* 2022, 61, 20253–20267



Read Online

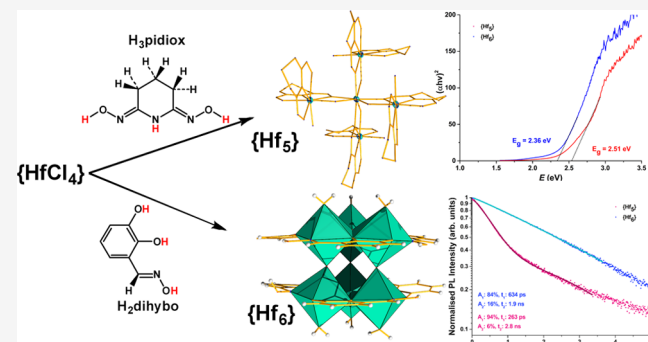
ACCESS |

 Metrics & More

 Article Recommendations

 Supporting Information

ABSTRACT: Hafnium(IV) molecular species have gained increasing attention due to their numerous applications ranging from high-resolution nanolithography, heterogeneous catalysis, and electronics to the design of molecule-based building blocks in metal–organic frameworks (MOFs), with applications in gas separation, sorption, luminescence sensing, and interim storage of radioactive waste. Despite great potential, their chemistry is relatively underdeveloped. Here, we use strong chelators ($2Z$ - $6Z$)-piperidine-2,6-dione (H_3 pidiox) and 2,3-dihydroxybenzaldehyde oxime (H_3 dihybo) to synthesize the first ever reported pentanuclear $\{Hf_5/H_3$ pidiox $\}$ and hexanuclear $\{Hf_6/H_3$ dihybo $\}$ clusters (HfOCs). The $\{Hf_n\}$ clusters adopt unique core structures $[Hf_6^{IV}(\mu_3-O)_2(\mu-O)_3]$ with a trigonal-prismatic arrangement of the six hafnium atoms and have been characterized via single-crystal X-ray diffraction analysis, UV–vis spectroscopy in the solid state, NMR, fluorescence spectroscopy, and high-resolution mass spectrometry in solution. One-dimensional (1D) and two-dimensional (2D) 1H NMR and mass spectroscopies reveal the exceptional thermodynamic stability of the HfOCs in solution. Interestingly, the conjunction of the oxime group with the catechol resulted in the remarkable reduction of the clusters’ band gap, below 2.51 eV. Another prominent feature is the occurrence of pronounced metalloaromaticity of the triangular $\{Hf_3\}$ metallic component revealed by its NICS_{zz} scan curve calculated by means of density functional theory (DFT). The NICS_{zz}(1) value of -44.6 ppm is considerably higher than the -29.7 ppm found at the same level of theory for the benzene ring. Finally, we investigated the luminescence properties of the clusters where **1** emits light in the violet region despite the lack of fluorescence of the free H_3 pidiox ligand, whereas the $\{Hf_6\}$ **3** shifts the violet-emitting light of the H_3 dihybo to lower energy. DFT calculations show that this fluorescence behavior stems from ligand-centered molecular orbital transitions and that Hf^{IV} coordination has a modulating effect on the photophysics of these HfOCs. This work not only represents a significant milestone in the construction of stable low-band-gap multinuclear Hf^{IV} clusters with unique structural features and metal-centered aromaticity but also reveals the potential of Hf(IV) molecule-based materials with applications in sensing, catalysis, and electronic devices.



INTRODUCTION

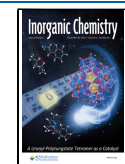
Group IV metal oxo clusters (MOCs) are polynuclear compounds exhibiting an inorganic core formed by group IV metals in their highest oxidation state linked by oxygen atoms and stabilized by capping ligands. Although there are many reported applications of group IV MOCs,^{1–8} their chemistry is still underdeveloped^{9–13} and particularly the hafnium chemistry in marked contrast to the titanium and zirconium. HfOCs have potential applications in high-resolution nanolithography,^{14–16} in heterogeneous catalysis,¹⁷ and they have been used as molecule-based building blocks in metal–organic frameworks (MOFs), with applications in gas separation,^{18,19}

sorption,²⁰ catalysis,^{21–28} luminescence sensing,²⁹ and interim storage of radioactive waste.³⁰

In addition, the study of HfOCs is of fundamental importance because they are processable molecular analogues of HfO_2 which have numerous applications including protective surface coatings,³¹ metal-oxide-semiconductor

Received: May 23, 2022

Published: December 3, 2022

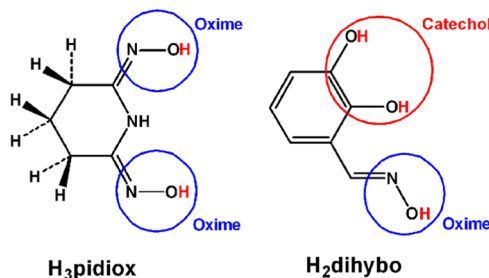


field-effect transistors,^{32,33} random access memory devices,^{34–37} and teeth prosthetics.³⁸

The band gap energy of HfO_2 ranges from 5.3 to 6.0 eV depending on its different phases and its formation under different experimental conditions.³⁹ This large band gap is practically prohibitive for the utilization of HfO_2 in photocatalytic applications. The modulation of the band gap can be achieved by employing organic chelators^{40–42} leading to visible light absorption by HfOCs .

Recently, our group studied the reaction of MCl_4 ($\text{M} = \text{Ti}^{\text{IV}}$, Zr^{IV}) with the organic ligands (2Z,6Z)-piperidine-2,6-dione dioxime (H_3pidiox)^{43,44} and 2,3-dihydroxybenzaldehyde (H_3dihybo) (Scheme 1).⁴⁰ Both ligands are strong binders

Scheme 1. Ligands H_3pidiox and H_3dihybo



to hard metals in their highest oxidation state,^{45,46} and have been used for the extraction of heavy hard metal ions from seawater.^{47–49} The employment of H_3pidiox and H_3dihybo led to the formation of polynuclear clusters with unique structural features, allowing the induction of metalloc aromaticity and the modulation of the compounds' band gap. The reaction of HfCl_4 with the ligand H_3dihybo gave a hexanuclear cluster, $\{\text{Hf}_6\}$, with two cyclo- $\{\text{Hf}_3\}$ metallic cores which exhibit metalloc aromaticity.

The discovery of the aromatic nature of benzene had a great impact on many fields of science such as organic, industrial, and medicinal chemistry, and life sciences.⁵⁰ The extensive investigation of metalloc aromaticity that took place in the last few years, led to a better understanding of the concept and exponential growth of examples in the literature⁵¹ due to the discovery of new metalloc aromatic species such as metalloc benzenes⁵² and all-metal clusters [i.e., (Al_4^{2-}) , (Au_5Zn^+) ⁵⁴]. Owing to the clusters' metalloc aromaticity-induced wide range of applications^{50,55–57} such as catalysis, drugs, molecular electronic devices, aerospace engineering, molecular magnets, the revelation of unknown aspects of chemical bonding, and understanding the electronic and surface properties of metal oxides, and mixed-metal clusters, this family of compounds has attracted the attention of numerous research groups. Metalloc aromaticity of all-metal cyclic species is due to the formation of σ , π , δ , and φ molecular orbitals (MOs),⁵⁰ in marked contrast to the organic aromatic rings where electron delocalization is supported by π MOs only.⁵⁰ Manifestation of metalloc aromatic behavior has been evaluated using several different criteria that have been developed over the years that are directly related to structural, energetic, magnetic, and electronic characteristics of the reported species. Among them, the magnetic nucleus-independent chemical shift (NICS) criterion appears to be one of the most powerful.⁵⁸ Therefore, in this work, we employ the NICS criterion to investigate whether the cyclic trinuclear $\{\text{Hf}_3\}$ metallic ring cores of the

newly synthesized compounds exhibit metalloc aromatic behavior.

Based on the above observations, our work is inspired by the prospect of generating new building units for the construction of metal–organic frameworks with potential application in catalysis, sensing, and gas separation. Moreover, the combination of the inherent inertness of Hf species and higher stabilities compared to first-row transition metals along with the highly polarized Hf–X bonds will potentially influence the catalytic, optoelectronic, and luminescence sensing applications. Herein, we report the synthesis, structure, and physicochemical characterization of the pentanuclear HfOC $[\text{Hf}_5(\mu\text{-OH})_4(\text{OH}_2)_4(\mu\text{-}\eta^1,\eta^1,\eta^2\text{-Hpidiox-O,N,O'})_4(\eta^1,\eta^1,\eta^1\text{-Hpidiox-O,N,O'})_4]\text{-KCl}\cdot 3.25\text{CH}_3\text{OH}\cdot 16.5\text{H}_2\text{O}$ (1) and of three hexanuclear HfOCs with general formula $[\text{Hf}_6(\mu_3\text{-O})_2(\mu\text{-O})_3(\text{OH}_2)_6(\mu\text{-}\eta^1,\eta^2,\eta^1\text{-Hdihybo-O,O',N})_6]$ (2–4) with the organic chelators H_3pidiox and H_3dihybo . HfOC 1 is the first example of a pentanuclear hafnium cluster to be reported.⁹ Both the core structure $[\text{Hf}_6(\mu_3\text{-O})_2(\mu\text{-O})_3]$ and the trigonal-prismatic arrangement of the six hafnium atoms in compounds 2–4 are unique. Moreover, the ligation of H_3pidiox and H_3dihybo ligands to Hf^{IV} induces fluorescence in solution at room temperature, rendering these $\text{Hf}/\text{H}_3\text{pidiox}/\text{H}_3\text{dihybo}$ clusters highly promising candidates for applications in sensing, catalysis, and optoelectronics.^{59–62}

EXPERIMENTAL SECTION

Synthesis of the HfOCs 1–4. *Experimental Details.* All chemicals and solvents purchased from Sigma-Aldrich and Merck were of reagent grade and used without further purification. C, H, and N analyses were conducted by the microanalytical service of the School of Chemistry, the University of Glasgow. Samples for EA were collected after the removal of the single crystals from the mother liquor by filtration and dried on the bench for 2 days.

Synthesis of $[\text{Hf}_5(\mu\text{-OH})_4(\text{OH}_2)_4(\mu\text{-}\eta^1,\eta^1,\eta^2\text{-Hpidiox-O,N,O'})_4(\eta^1,\eta^1,\eta^1\text{-Hpidiox-O,N,O'})_4]\text{-KCl}\cdot 3\text{CH}_3\text{OH}\cdot 16\text{H}_2\text{O}$ (1). To a stirred moist methyl alcohol solution (4 mL) were successively added H_3pidiox (89.3 mg, 0.624 mmol) and HfCl_4 (100 mg, 0.312 mmol). Then, upon addition of one portion of solid KOH (35 mg, 0.624 mmol), a white precipitate was formed which was filtered off and the colorless filtrate was kept at room temperature ($\sim 20^\circ\text{C}$) for 5–6 days, during which period white crystals were formed. The crystals were filtered to obtain 98.6 mg of HfOC 1. (Yield: 60%, based on HfCl_4). Anal. Calcd for $(\text{C}_{40}\text{H}_{92}\text{N}_{24}\text{O}_{24}\text{Hf}_5)\text{-KCl}\cdot 3\text{CH}_3\text{OH}\cdot 16\text{H}_2\text{O}$, $M_r = 2602.42 \text{ g mol}^{-1}$): C 19.85, H 3.64, N 12.92; found: C 19.63, H 4.31, N 12.72.

Synthesis of $[\text{Hf}_6^{\text{IV}}(\mu_3\text{-O})_2(\mu\text{-O})_3(\text{OH}_2)_6(\mu\text{-}\eta^1,\eta^2,\eta^1\text{-Hdihybo-O,O',N})_6]\text{-Cl}_2\cdot (\text{Et}_3\text{NHC})\cdot 2\text{CH}_3\text{OH}\cdot 1.5\text{H}_2\text{O}$ (2). To a stirred moist methyl alcohol solution (4 mL) were successively added H_3dihybo (47.8 mg, 0.312 mmol) and HfCl_4 (100.0 mg, 0.312 mmol). The colorless solution of the ligand turned light orange upon addition of HfCl_4 . Then, 1.6 mL of tetrabutylammonium hydroxide, 0.39 M in methyl alcohol (162.0 mg, 0.624 mmol) was added in one portion. The solution was filtered and a light orange filtrate was obtained and was kept at room temperature ($\sim 20^\circ\text{C}$) for 4–5 days, during which period yellow crystals were formed. We were unable to prepare an analytically pure sample on a preparative scale because the compound is very hygroscopic. Even though single crystals were also obtained in this case, the data were not of publishable quality due to the hygroscopic nature of the single crystal but allowed us to determine the content of the unit cell (see Figure S1) and provide the formula above.

$[\text{Hf}_6^{\text{IV}}(\mu_3\text{-O})_2(\mu\text{-O})_3(\text{OH}_2)_6(\mu\text{-}\eta^1,\eta^2,\eta^1\text{-Hdihybo-O,O',N})_6]\text{-Cl}_2\cdot (\text{Et}_3\text{NHC})\cdot 2\text{CH}_3\text{OH}\cdot 1.5\text{H}_2\text{O}$ (3). To a stirred moist methyl alcohol solution (4 mL) were successively added H_3dihybo (47.8 mg, 0.312 mmol) and HfCl_4 (100.0 mg, 0.312 mmol). The colorless solution of the ligand turned light orange upon addition of HfCl_4 . Then,

triethylamine (0.087 mL, 0.624 mmol) was added in one portion. The solution was stirred for 5 min, filtered, and the light orange filtrate was obtained and was kept at room temperature ($\sim 20^\circ\text{C}$) for 4–5 days, during which period yellow crystals were formed. The crystals were filtered to obtain 103 mg of HfOC 3. (Yield: 82%, based on HfCl_4) Anal. Calcd for $((\text{C}_{42}\text{H}_{48}\text{N}_6\text{O}_{29}\text{Hf}_6\text{Cl}_2 \cdot (\text{Et}_3\text{NHCl}) \cdot 2\text{CH}_3\text{OH} \cdot 1.5\text{H}_2\text{O})$, $M_r = 2470.355$ g mol⁻¹): C 24.31, H 2.69, N 3.97; found: C 23.85, H 2.70, N 4.02.

$\{[\text{Hf}_6^{\text{IV}}(\mu_3\text{-O})_2(\mu\text{-O})_3(\text{OCH}_3)_2(\text{OH}_2)_4(\mu\text{-}\eta^1, \eta^2, \eta^1\text{-Hdihybo-O, O', N})_6]\text{Cl}_2\text{C}_5\text{H}_5\text{N}\cdot\text{CH}_3\text{OH}\cdot 5\text{H}_2\text{O}$ (4). To a stirred moist methyl alcohol solution (4 mL) were successively added H_3dihybo (47.8 mg, 0.312 mmol) and HfCl_4 (100.0 mg, 0.312 mmol). The colorless solution of the ligand turned light orange upon addition of HfCl_4 . Then, pyridine (0.05 mL, 0.624 mmol) was added in one portion. The solution was stirred for 5 min, filtered, and the light orange filtrate was kept at room temperature ($\sim 20^\circ\text{C}$) for 4–5 days, during which period yellow crystals were formed. The crystals were filtered to obtain 93 mg of HfOC 4. (Yield: 75%, based on HfCl_4) Anal. Calcd for $(\text{C}_{42}\text{H}_{42}\text{N}_6\text{O}_{29}\text{Hf}_6\text{Cl}_2 \cdot \text{C}_5\text{H}_5\text{N}\cdot\text{CH}_3\text{OH}\cdot 5\text{H}_2\text{O})$, $M_r = 2449.88$ g mol⁻¹): C 24.02, H 2.51, N 4.00; found: C 23.81, H 2.49, N 4.07.

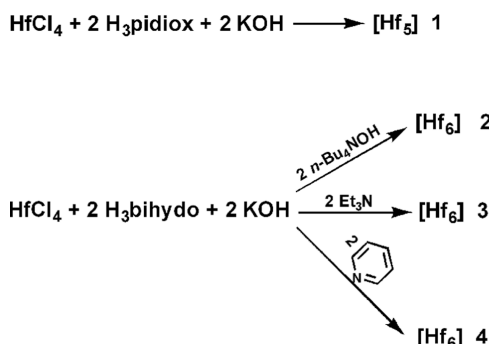
Computational Details. The Amsterdam Density Functional⁶³ (ADF 2019.304) program suite was used for the calculation of excited state geometries. The revised⁶⁴ Perdew, Burke, and Ernzerhof⁶⁵ gradient corrected density functional with Grimme's fourth generation dispersion correction⁶⁶ (revPBE-D4) was used together with a Slater type basis set of triple zeta quality augmented with an additional polarization function (TZP). The COSMO⁶⁷ implicit solvation scheme was also employed with the default parameters for methanol. Due to the presence of heavy elements, the scalar Zero Order Regular Approximated (ZORA) Hamiltonian⁶⁸ was applied in the optimization runs. Geometry optimizations were performed on the $\{\text{Hf}_5\}$ and $\{\text{Hf}_6\}$ molecular models constrained to the C_2 point group symmetry to allow for Jahn–Teller distortions in the excited state. Vertical excited state energies were computed with the spin-orbit perturbative approach (SOPERT) of the time-dependent⁶⁹ density functional (TD-revPBE-D4) and these showed no changes in either transition energy or oscillator strengths relative to the spin-free wavefunctions. We found that this approach affords a reasonable compromise between accuracy and computational performance.

The calculation of the NICS values employed the gauge-including atomic orbital (GIAO) DFT method^{70,71} as implemented in the Gaussian09 series of programs⁷² employing the PBE0 functional in combination with the 6-31G(d,p) basis set for all nonmetal atoms, E and the Def2-TZVP basis set for Hf atoms (the computational protocol is denoted as GIAO/PBE0/Def2-TZVP(Hf)U6-31G(d,p)-(E)).

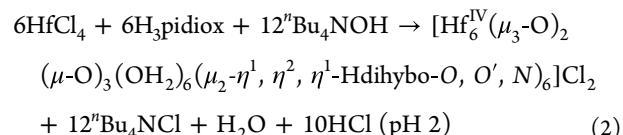
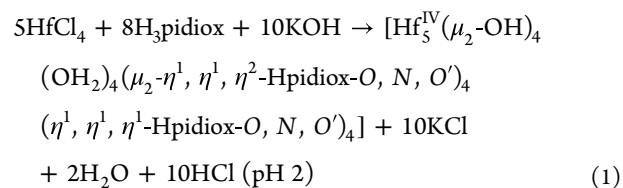
RESULTS AND DISCUSSION

Synthesis of the HfOCs 1–4. Pentanuclear HfOC/ H_3pidiox 1 was synthesized via a one-pot three-component reaction (eq 1 and Scheme 2) at room temperature, while the

Scheme 2. Synthesis of HfOCs 1 $\{\text{Hf}_5\}$, 2, 3, and 4 $\{\text{Hf}_6\}$



hexanuclear HfOCs/ H_3dihybo 2, 3, and 4 (eq 2 and Scheme 2) were also synthesized in a similar fashion. When KOH was used as a base in the reaction mixture of HfCl_4 with H_3dihybo , no suitable crystals for X-ray structure analysis of $\{\text{Hf}_6\}$ were obtained, while the use of ${}^n\text{Bu}_4\text{NOH}$ led to hygroscopic $\{\text{Hf}_6\}$ 2. Finally, the use of Et_3N and pyridine resulted in the isolation of $\{\text{Hf}_6\}$ HfOCs 3 and 4, respectively, which were suitable for physicochemical measurements.



Crystal Structures. The structure of HfOC 1 contains a pentanuclear hafnium(IV) core supported by four chelate Hpidiox²⁻ ligands, four chelate-bridging Hpidiox²⁻ and four $\mu_2\text{-OH}^-$ groups (Figure 1A). Interestingly, the $\{\text{Hf}_5^{\text{IV}}\}$ cluster is the only single pentanuclear hafnium(IV) cluster reported so far.⁹ The four outer hafnium(IV) atoms adopt a distorted tetrahedral arrangement (Figure 1B). In the center of the $\{\text{Hf}_4^{\text{IV}}\}$ tetrahedron is located the fifth hafnium(IV) atom, Hf(4) (Figure 1B), bound by four μ -bridging oxime oxygen atoms and four $\mu_2\text{-OH}^-$ groups in a bi-capped distorted O_8 coordination (Figure 1A,C-I). The four outer hafnium(IV) atoms also adopt a bi-capped distorted N_2O_6 ligation (Figure 1C-II). Based on bond valence sum (BVS) calculations, the valences of O(17), O(18), O(19), and O(20) atoms were found to be close to 2 after considering a proton attached to each oxygen atom. BVS calculations for the terminal oxygen atoms O(21), O(22), O(23), and O(24) (Figure 2) revealed that they are doubly protonated (aqua ligands). The $\text{Hf}^{\text{IV}}\text{-OH}_2$ bond lengths are 2.192 ± 0.003 Å. The central hafnium(IV) atom, Hf(4), shows two sets of $\text{Hf}(4)^{\text{IV}}\text{-O}$ bonds with mean $\text{Hf}(4)^{\text{IV}}\text{-O}$ bond lengths of 2.159 ± 0.007 Å for the bridging $\mu\text{-OH}^-$ groups and 2.21 ± 0.01 Å for the bridging oxime $\mu\text{-O}^-$ atoms (Figure 2).

The X-ray crystallographic study of HfOC 3, which crystallizes in a centrosymmetric space group and the unit cells contain a hexanuclear molecular structure (Figure 3A). The core structure of the hexanuclear $\{\text{Hf}_6\}$ hafnium(IV) cluster is formed from two $[\text{Hf}_3^{\text{IV}}(\mu_3\text{-O})]$ subunits, which are connected by three $\mu\text{-O}^{2-}$ bridges with the six hafnium(IV) atoms in a trigonal-prismatic arrangement (Figure 3B). The $\{\text{Hf}_3^{\text{IV}}\}$ subunits are supported by three chelate-bridging doubly deprotonated Hdihybo²⁻ ligands (Figure 3C).

The only hexanuclear HfOCs $\{\text{Hf}_6\}$ reported thus far that incorporate six metal atoms in three different structural arrangements are shown in Figure S2; more specifically: the octahedral (Figure S2A),⁷³ the star-shaped cyclic planar (Figure S2B),⁷⁴ and the cyclic planar (Figure S2C)⁷⁵ arrangements of the six hafnium atoms. Thus, the trigonal-prismatic arrangement of the six hafnium atoms found in 3 is unique.

The $\mu_3\text{-O}^{2-}$ is located $0.489(4)$ Å above the plane defined by the three hafnium(IV) atoms Hf(1)–Hf(2)–Hf(3) (Figure

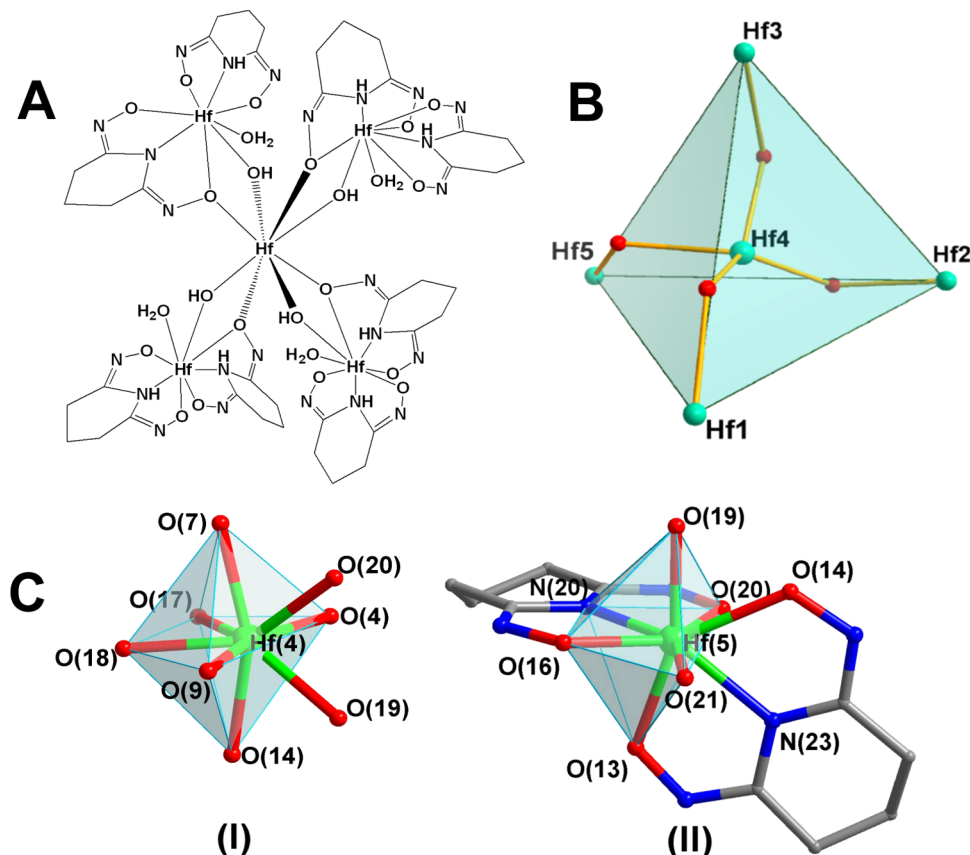


Figure 1. (A) Molecular drawing of the neutral pentanuclear HfOC **1**, $[\text{Hf}_5(\mu\text{-OH})_4(\mu\text{-Hpidiox})_4(\text{Hpidiox})_4]$. (B) Tetrahedral arrangement of $[\text{Hf}_5^{IV}(\mu\text{-OH})_4]$. (C) The bi-capped octahedral coordination environment of Hf(4) (**I**) and Hf(5) (**II**) atoms in **1**.

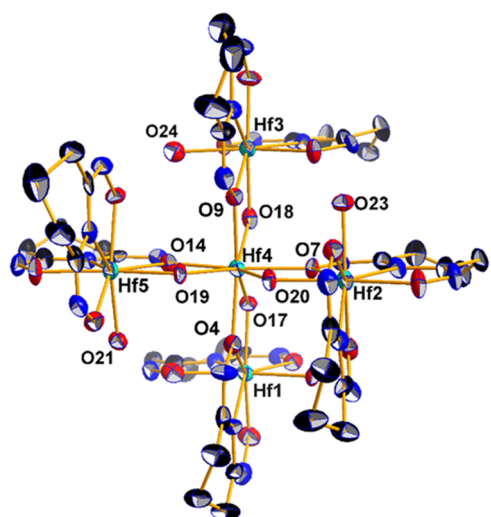


Figure 2. Oak Ridge thermal ellipsoid plot (ORTEP) (50% probability level) of the neutral pentanuclear HfOC **1**, with a partial labeling scheme. Hydrogen atoms and co-crystallized solvent molecules have been omitted for clarity.

3B). The distances between the three Hf atoms bridged by the $\mu_3\text{-O}^{2-}$ atom is 3.455 ± 0.004 Å. The distance between the two trigonal planes defined by Hf(1)–Hf(2)–Hf(3) and atoms Hf(4)–Hf(5)–Hf(6) is 3.866 (4) Å. The $\text{Hf}^{IV}\text{-}\mu_3\text{-O}^{2-}$ bond lengths are 2.053 ± 0.003 Å, while the Hf– $\mu\text{-O}^{2-}$ bond lengths are 1.929 ± 0.002 Å. The three angles in the symmetry-related Hf_3^{IV} triangles are almost 60° , and thus, it is obvious that the

Hf_3^{IV} triangles are equilateral. The $d(\text{Hf}^{IV}\text{-O}_{\text{cat}}^-)_{\text{av}}$ and $d[\text{Hf}^{IV}\text{-}(\mu\text{-O}_{\text{cat}})]_{\text{av}}$ values are 2.120(4) and 2.217(4) Å, respectively, and are very close to those reported in the literature.⁷⁶ The doubly deprotonated catecholate moiety adopts a singly bridging chelate $\mu\text{-}(O,O',O')$ mode of coordination. The $d(\text{Hf}^{IV}\text{-N}_{\text{ox}})_{\text{av}}$ value of 2.384(6) Å is much higher than the reported mean value of 2.187(8) Å,⁷⁷ but in the latter case, the oxime is deprotonated and acts as a $\mu_2\text{-}\eta^1,\eta^2\text{-}N,O^-$ bridging ligand. Compound **3** is the first example of a polyoxocatecholate hafnium(IV) compound reported to date.

HfOCs **2** and **4** contain identical $\{\text{Hf}_6\}$ structural units to cluster **3**. Thus, only the structural features of compound **3** are discussed in detail (vide supra). In the case of HfOC **2**, its structure was not possible to be finalized due to severe disorder of the tetrabutyl ammonium counterions as can be seen in Figure S1. Nevertheless, the remaining part of the structure is well resolved. Additionally, the X-ray structure analysis of **4** revealed a unit cell with two $\{\text{Hf}_6\}$ clusters, where one of them was found to accommodate two methoxy terminal ligands and four aqua ligands instead of six aqua ligands (Figure S3). The structural features of **4**'s metallic core are identical to those of **3**.

Solid-State UV-Vis Spectroscopy. Figure 4 shows the solid-state UV-vis spectra of HfOCs **3** and **4**, while the solution (MeOH) UV-vis spectra of **1** and **3** are shown in Figures S4–S6. In solution, **1** and **3** absorb in the UV region up to 360 and 500 nm, respectively. In the solid state the absorption of **3** and **4** shifts to lower energy up to 800 nm due to the intermolecular interactions. The band gaps for

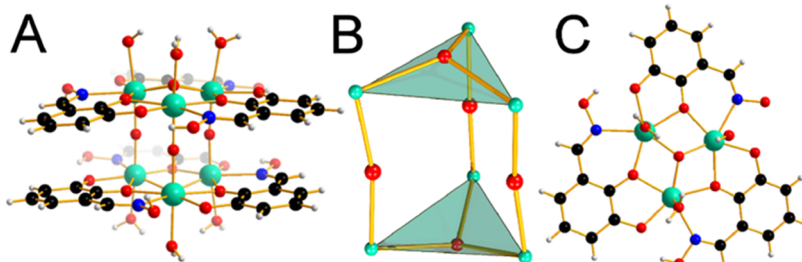


Figure 3. Ball-and-stick plot of cation of **3** (A). The trigonal-prismatic arrangement of the six hafnium(IV) atoms in the cluster core $\{ \text{Hf}_6^{\text{IV}}\text{O}_5 \}$ (B) Ball-and-stick plot of the structural unit $[\text{Hf}_3^{\text{IV}}(\mu_3\text{-O})(\mu\text{-}\eta^1\text{:}\eta^2\text{:}\eta^1\text{-Hdihybo-}\text{O},\text{O}',\text{N})_3(\text{OH}_2)_3]$ (C).

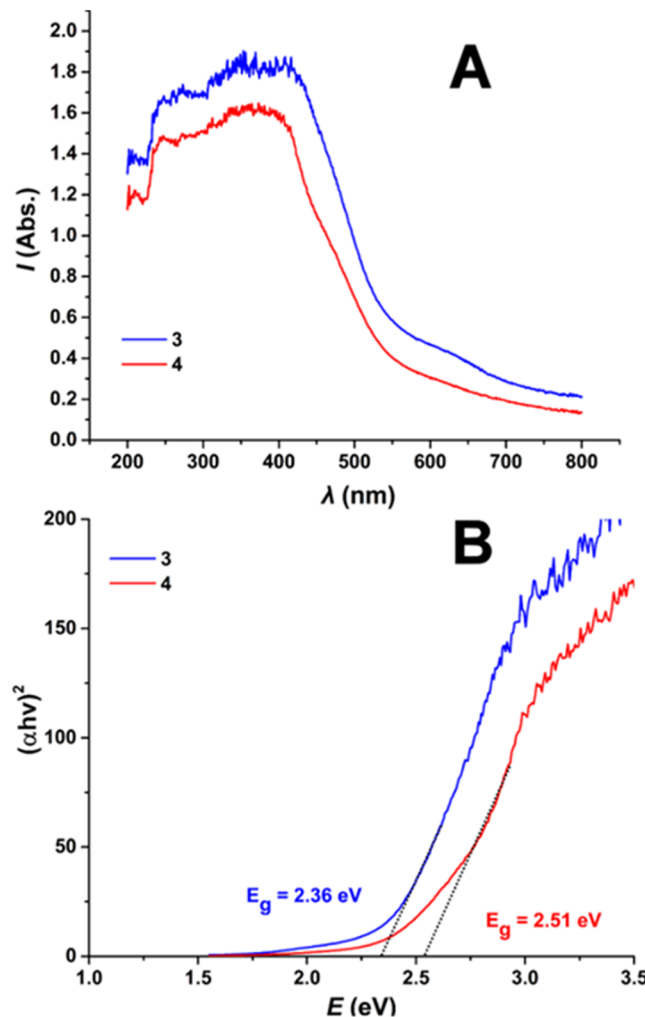


Figure 4. (A) UV-vis reflectance spectra of HfOCs **3** and **4**. (B) Tauc plots of HfOCs **3** and **4**.

compounds **3** and **4** were found to be 2.36 and 2.51 eV, respectively, and were calculated from the solid-state spectra employing the Kubelka–Munk method.⁷⁸ Interestingly, HfOCs **3** and **4** revealed substantially low band gap values rendering the Hf-based molecular species highly promising candidates for semiconducting photocatalytic applications. This finding demonstrates the constructive co-operative effect of the catechol and oxime moieties not only in stabilizing unique structural features but also in modifying the clusters' electronic structure by substantially reducing the band gap value in comparison to $\text{Hf}^{\text{IV}}\text{O}_2$. This observation paves the way for the discovery of new HfOCs by exploiting the stabilizing

effect of organic ligands that incorporate appropriate coordinating moieties.

NMR Spectroscopy. The ^1H and ^{13}C NMR chemical shifts of the ligand H_3pidiox and the pentanuclear hafnium(IV)

Table 1. ^1H and ^{13}C Chemical Shifts (ppm) of the Pentanuclear Cluster **1** and the Ligand H_3pidiox

	1		H_3pidiox	
	^{13}C	^1H ^a	^{13}C	^1H ^a
C(2,4)	20.30	2.7271	26.20	2.3670
C(3)	17.97	2.0569	19.31	1.7111
C(1,5)	156.42		148.57	

^aThe chemical shifts of the protons are measured at the center of the observed multiplets.

cluster **1** in solution (CD_3OD) are collected in Table 1. The ^1H NMR spectrum of the ligand H_3pidiox (Figure 5) shows

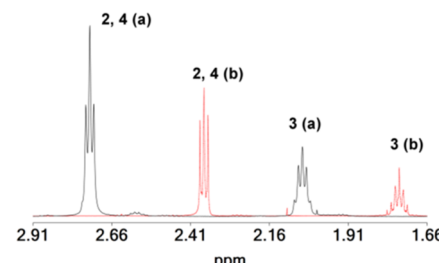
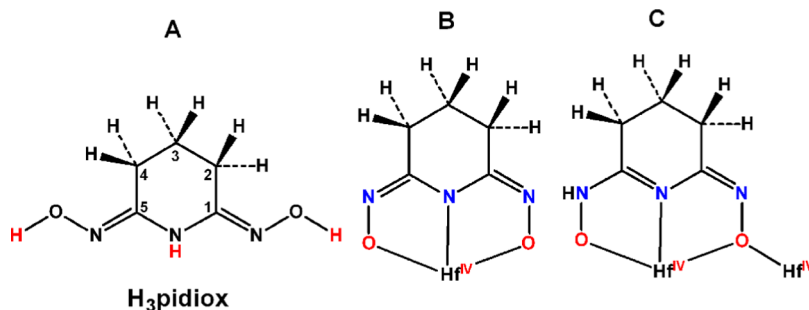


Figure 5. ^1H NMR spectra in solution (CD_3OD) of the pentanuclear cluster **1** (in black color) and of the H_3pidiox ligand (in red color).

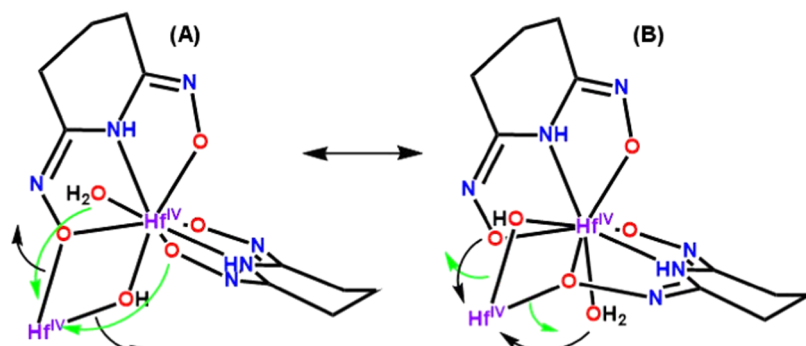
one quintet and one triplet at 1.71 and 2.37 ppm assigned to the two protons attached to C(3) and the four protons attached to {C(2), C(4)}, respectively (Scheme 3A), while its ^{13}C NMR spectrum gave three peaks at 19.32, 26.20, and 148.57 ppm assigned to C(3), {C(2), C(4)}, and {C(1), C(5)}, respectively.

The X-ray diffraction analysis of **1** (Figures 1A and 2) revealed the existence of chelate (Scheme 3B) and chelate/bridging (Scheme 3C) modes of ligation of the ligand Hpidiox^{2-} . However, the ^1H and ^{13}C NMR spectra of **1** exhibit only one set of peaks. This might be attributed to a fast exchange between the ligands with a different coordination mode. A dynamic structural change between the chelate and chelate/bridging modes can occur intramolecularly by a simple breaking of the $\text{Hf}(1)\text{--O}_{\text{oxime/bridging}}$ bond (Scheme 4A) and the formation of an $\text{Hf}(1)\text{--O}_{\text{oxime/terminal}}$ bond (Scheme 4B) and vice versa.

Scheme 3. Numbering of the Carbon Atoms of the Ligand H₃pidiox (A) and the Two Modes of Ligation (B, C) of Hpidiox²⁻ in 1



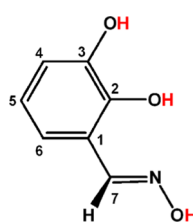
Scheme 4. Dynamic Equilibrium between the Chelate/Bridging and Chelate Ligation Modes of the Ligand Hpidiox²⁻ in A from Chelate to Chelate/Bridging in B and Vice Versa



The ¹³C NMR peaks of the carbon atoms 2, 4, and 3 in cluster 1 [identified in two-dimensional (2D) {¹H, ¹³C} grHSQC spectrum, Figure S7] shift to a higher field, 17.97 ppm C(3), 20.30 ppm C(2, 4), and of C(1, 5) [156.42, identified in the 2D {¹H, ¹³C} grHMBC spectrum (Figure S8)] to a lower field compared with the chemical shifts of the free ligand (Table 1).

The ¹H and ¹³C NMR peaks of the free ligand are also shifted in the hexanuclear HfOCs 3 or 4 due to the ligation of Hdihybo²⁻ to the Hf^{IV} metal centers. The coordination of the metal ion to the oxime nitrogen atom induces deshielding of C(7) (Scheme 5) for 3 (0.3 ppm, Table 2).

Scheme 5. Numbering of the Carbon Atoms of the H₃dihybo Ligand



The ligand's H₃dihybo neighboring protons of 3 in solution (CD₃OD) [H(7)-H(6), H(6)-H(5), H(5)-H(4)] show strong NOESY interaction in 2D {¹H} nuclear Overhauser effect spectroscopy (NOESY)-exchange spectroscopy (EXSY) spectra. Weaker NOESY off-diagonal peaks (Figure 6) are observed between the protons H(7)-H(4), H(7)-H(5), and H(4)-H(6) assigned to intra-ligand proton interactions between the protons of the ligands belonging to the two [M₃(Hdihybo)₃] planes as depicted for HfOC 3 in Figure 6. The distances between protons 4–7, based on the intensity of

Table 2. ¹³C [¹H] NMR Chemical Shifts for H₃dihybo and 3 and the Shielding/Deshielding Effect ($\Delta\delta$, ppm) upon Complexation

	H ₃ dihybo	3/ $\delta^{13}\text{C}^a$ ($\Delta\delta^b$) [$\delta^1\text{H}$ ($\Delta\delta^b$)]
C(1)	117.6	
C(2)	146.5	
C(3)	146.4	
C(4)	120.4 [6.80]	120.5 (+0.1) [6.804 (+0.004)]
C(5)	118.8 [6.72]	122.0 (+3.2) [6.674 (-0.046)]
C(6)	121.7 [6.76]	124.5 (+2.8) [6.231 (-0.529)]
C(7)	152.3 [8.19]	152.6 (+0.3) [7.781 (-0.410)]

^aThe ¹³C NMR chemical shifts of 3 were found from the 2D {¹H, ¹³C} grHSQC spectrum. ^b $\delta_{\text{M-L}} - \delta_{\text{L}}$.

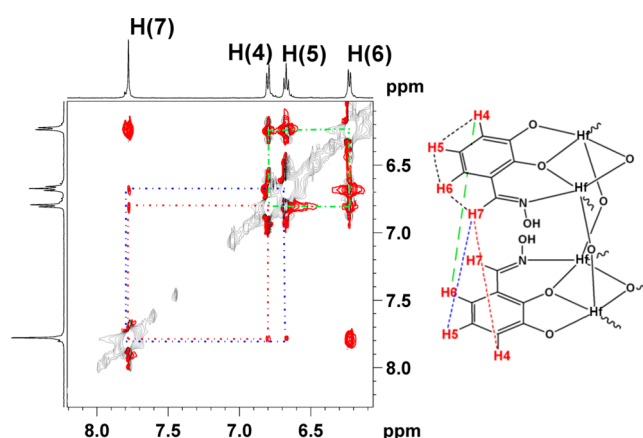


Figure 6. Two-dimensional (2D) {¹H} NOESY spectrum of HfOC 3 and the assignments of the NOESY interactions.

Table 3. Representation of the Experimentally Identified and Simulated *m/z* Values of the Distribution Envelopes of {Hf₅} Cluster 1

exp.	theor.	charge	formula
1528.96	1529.04	-1	{Hf ₄ ^{IV} (C ₅ N ₃ O ₂ H ₆) ₂ (C ₅ N ₃ O ₂ H ₅) ₂ K(OCH ₃) ₇ } ⁻
1565.93	1566.07	-1	{Hf ₄ ^{IV} (C ₅ N ₃ O ₂ H ₆) ₃ (C ₅ N ₃ O ₂ H ₅)K(OH ₂) ₂ (OCH ₃) ₇ } ⁻
1584.92	1585.08	-1	{Hf ₄ ^{IV} (C ₅ N ₃ O ₂ H ₆) ₄ K(OH ₂) ₃ (OCH ₃) ₇ } ⁻
1602.90	1603.09	-1	{Hf ₄ ^{IV} (C ₅ N ₃ O ₂ H ₆) ₄ K(OH ₂) ₄ (OCH ₃) ₇ } ⁻
1155.96	1155.92	-2	{Hf ₅ ^{IV} (C ₅ N ₃ O ₂ H ₆) ₄ (C ₅ N ₃ O ₂ H ₅) ₄ (OH) ₄ K ₆ } ²⁻
1173.95	1173.93	-2	{Hf ₅ ^{IV} (C ₅ N ₃ O ₂ H ₆) ₄ (C ₅ N ₃ O ₂ H ₅) ₄ (OH) ₄ K ₆ (OH ₂) ₂ } ²⁻
1191.94	1191.94	-2	{Hf ₅ ^{IV} (C ₅ N ₃ O ₂ H ₆) ₄ (C ₅ N ₃ O ₂ H ₅) ₄ (OH) ₄ K ₆ (OH ₂) ₄ } ²⁻
1211.92	1211.97	-2	{Hf ₅ ^{IV} (C ₅ N ₃ O ₂ H ₆) ₈ (OH) ₄ K ₆ (OH ₂) ₆ } ²⁻
1229.90	1229.98	-2	{Hf ₅ ^{IV} (C ₅ N ₃ O ₂ H ₆) ₄ (OH) ₄ K ₆ (OH ₂) ₈ } ²⁻
1248.38	1248.50	-2	{Hf ₆ ^{IV/III} (C ₅ N ₃ O ₂ H ₆) ₈ H(OH) ₄ K ₆ (OH ₂) ₁₀ } ²⁻
1266.86	1267.00	-2	{Hf ₃ ^{IV} Hf ₂ ^{III} (C ₅ N ₃ O ₂ H ₆) ₈ H ₂ (OH) ₄ K ₆ (OH ₂) ₁₂ } ²⁻

the NOESY cross peaks, are H(7)–H(4) < H(4)–H(6) < H(7)–H(5), in agreement with the distances found in the crystal structure of HfOC 3. Apparently, HfOCs 3 and 4 retain their structural integrity in solution. The ¹H and ¹³C NMR spectra of HfOCs 3 and 4 in D₂O and CD₃OD are similar indicating that HfOCs 3 and 4 are hydrolytically stable.

Electrospray Ionization Mass Spectrometry (ESI-MS).

The characterization of the pentanuclear {Hf₅} cluster 1 in solution was carried out using high-resolution ESI-MS to determine the compound's stability in solution.⁷⁹ The ESI-MS studies were performed in methanol in negative ionization mode. The presence of higher-intensity isotopic distribution envelopes is due to the existence of the pentanuclear moiety, resulting from the combination of protons, counterions, and solvent molecules. Occasionally, the in situ induction of partial fragmentation during the course of ion transfer in addition to alteration of the metal's oxidation state is quite common and has been reported frequently in the literature.^{80,81} A series of doubly charged distribution envelopes that can be assigned to the intact {Hf₅} cluster (Figure S9) can be observed in the higher region of *m/z* values. In this case, a group of distribution envelopes are clustered within the range of ca. 1100–1300 *m/z*. More specifically, the central isotopic distribution envelope at 1191.95 *m/z* can be assigned to the {Hf₅^{IV}(C₅H₆N₃O₂)₈(OH)₄K₆(OH₂)₄}²⁻ anion which is flanked by isotopic envelopes of the same moiety associated with a different number of solvent molecules with the general formula of {Hf₅(C₅H₆N₃O₂)₈(OH)₄K₆(OH₂)_x}²⁻, where *x* = 0–12 (Table 3). A representative example of this group of species is the expanded distribution envelope shown in Figure S10 along with its simulated pattern, which corresponds to the intact {Hf₅} cluster. In the range of ca. 1500–1600 *m/z* values, another group of envelopes has been identified and assigned as a singly charged tetrameric cluster, which is due to the partial fragmentation of the {Hf₅} moiety which takes place during the ionization and ion transfer process^{80,81} with general formula {Hf₄^{IV}L₄K_y(OH₂)_z(OCH₃)₇}⁻, where *y* = 0, 1 and *z* = 0, 2, 3, or 4 (Table 3).

In a similar manner, the {Hf₆} cluster preserves its structural features in solution, as identified by a series of singly charged distribution envelopes (Figure 7). The assignment of the observed isotopic distribution envelopes reveals the main structural motif {Hf₃^{IV}Hf₂^{III}O₅(C₇H₅NO₃)₃(C₇H₄NO₃)₃}(solv)_x associated with different amalgamations of solvent molecules (H₂O or CH₃OH) coordinated or associated with the ionized {Hf₆} cluster, see Table 4 for a detailed assignment.

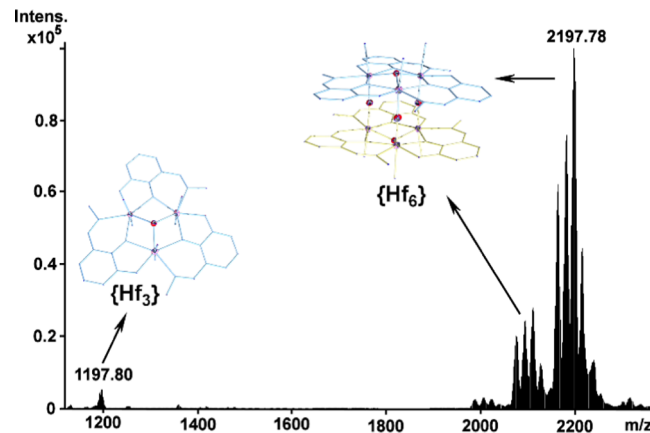


Figure 7. Negative ion mass spectrum of 3 exhibiting two characteristic sets of isotopic distribution envelopes centered at ca. 1179.80, 1183.80, and 1193.85 *m/z* with the formulae {Hf₅O-(C₇H₅NO₃)₂(C₇H₄NO₃)(OH₂)₇Cl(HOMe)}⁻, {Hf₃O-(C₇H₅NO₃)₂(C₇H₄NO₃)(OH₂)₈Cl}⁻, and {Hf₃O-(C₇H₅NO₃)₂(C₇H₄NO₃)(OH₂)₅Cl(HOMe)₂}⁻, respectively, and in the range of ca. 2000–2300 *m/z* with the general formula {Hf₆^{IV/III}O₅L₆(OH₂)_z(OCH₃)_{Cl₂H_w}}⁻, where *x* = 1–8, *y* = 0 or 1, *z* = 0 or 1, and *w* = 1–5.

In a similar fashion, the observation of changes in the metal's oxidation state is quite common as discussed above.

Interestingly, the lower *m/z* region (ca. 1000–1200 *m/z*) revealed the presence of the fundamental trimeric building block generated during the ionization process. The singly charged distribution envelopes centered at 1179.80, 1183.80, and 1193.85 *m/z* values demonstrate the presence of the Hf-oxo-centered triangles that can provide crucial information about the formation of these clusters. The identification of the trimeric building blocks indicates the formation of the trimeric clusters prior to their subsequent utilization as building blocks for the construction of the hexanuclear species that can be isolated as single crystals. Similar behavior has been observed in the solution studies conducted for the {Ti₆} and {Zr₆} species reported previously by our group.^{40,43} More specifically, we observed the {Hf₃O(C₇H₅NO₃)₂(C₇H₄NO₃)-(OH₂)₇Cl(HOMe)}⁻ (1179.80), {Hf₃O(C₇H₅NO₃)₂(C₇H₄NO₃)(OH₂)₈Cl}⁻ (1183.80), and {Hf₃O-(C₇H₅NO₃)₂(C₇H₄NO₃)(OH₂)₅Cl(HOMe)₂}⁻ (1193.85) Hf-based oxo-centered molecular triangles, as shown in Figure S11.

Metalloaromaticity of the Cyclic Trinuclear {Hf₃} Metallic Ring Cores of HfOC 3 {Hf₆}. Next, we set out to

Table 4. Representation of the Experimentally Identified and Simulated *m/z* Values of the Distribution Envelopes of {Hf₃} Cluster 3

exp.	theor.	charge	formula
2075.70	2075.81	-1	{Hf ₃ ^{IV} Hf ₃ ^{III} O ₅ (C ₇ H ₅ NO ₃) ₃ (C ₇ H ₄ NO ₃) ₃ (OH ₂)H ₃ } ⁻
2094.69	2094.83	-1	{Hf ₂ ^{IV} Hf ₄ ^{III} O ₅ (C ₇ H ₅ NO ₃) ₃ (C ₇ H ₄ NO ₃) ₃ (OH ₂) ₂ H ₄ } ⁻
2110.69	2110.83	-1	{Hf ₄ ^{IV} Hf ₂ ^{III} O ₅ (C ₇ H ₅ NO ₃) ₃ (C ₇ H ₄ NO ₃) ₃ (OH ₂) ₂ H ₂ } ⁻
2127.73	2127.83	-1	{Hf ₅ ^{IV} Hf ₂ ^{III} O ₅ (C ₇ H ₅ NO ₃) ₃ (C ₇ H ₄ NO ₃) ₃ (OH ₂) ₄ H} ⁻
2163.79	2163.89	-1	{Hf ^V Hf ₅ ^{III} O ₅ (C ₇ H ₅ NO ₃) ₃ (C ₇ H ₄ NO ₃) ₃ (OH ₂) ₄ (HOME)H ₅ } ⁻
2181.77	2181.89	-1	{Hf ^V Hf ₅ ^{III} O ₅ (C ₇ H ₅ NO ₃) ₃ (C ₇ H ₄ NO ₃) ₃ (OH ₂) ₅ (HOME)H ₅ } ⁻
2197.78	2197.89	-1	{Hf ₅ ^{IV} Hf ₃ ^{III} O ₅ (C ₇ H ₅ NO ₃) ₃ (C ₇ H ₄ NO ₃) ₃ (OH ₂) ₆ (HOME)H ₃ } ⁻
2214.78	2214.90	-1	{Hf ₄ ^{IV} Hf ₂ ^{III} O ₅ (C ₇ H ₅ NO ₃) ₃ (C ₇ H ₄ NO ₃) ₃ (OH ₂) ₇ (HOME)H ₂ } ⁻
2238.74	2238.87	-1	{Hf ₂ ^{IV} Hf ₄ ^{III} O ₅ (C ₇ H ₅ NO ₃) ₃ (C ₇ H ₄ NO ₃) ₃ (OH ₂) ₈ ClH ₅ } ⁻

study whether or not the cyclic trinuclear {Hf₃} metallic ring cores exhibit metalloaromaticity⁵⁰ and to probe the aromaticity/antiaromaticity of the rings, we employed the magnetic criterion, i.e., the nucleus-independent chemical shifts (NICS) by computing the NICS_{zz} scan curves.^{82–84} Accordingly, we calculated the NICS_{zz} scan curve of the *cyclo*-{Hf₃} trinuclear metallic core with the PBE0 functional that has been found to perform well in modeling molecular properties of heavy metals.⁸⁵ The NICS_{zz} curve is given in Figure 8, while the inset

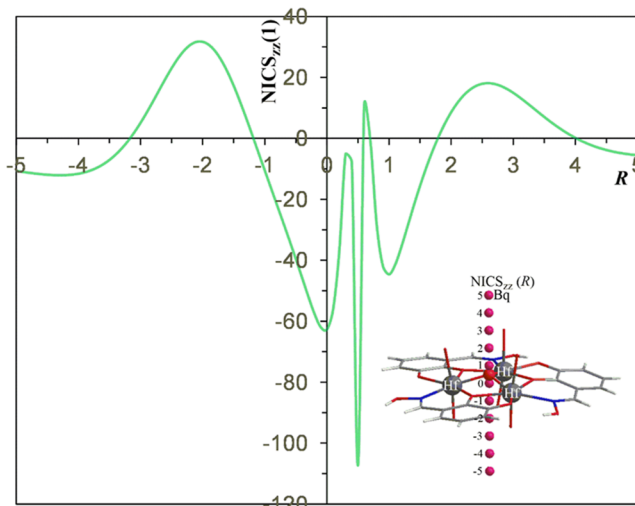


Figure 8. NICS_{zz}(*R*) (*R* in Å) scan profile of *cyclo*-{Hf₃} trinuclear core calculated at the GIAO/PBE0/Def2-TZVP(Hf)U6-31G(d,p)(E) level.

picture depicts the positions of the Bq ghost atoms. Sigma aromaticity arises from σ MOs delocalized in the plane of the ring, while π , δ , and ϕ arise from π , δ , and ϕ MOs delocalized over the ring plane, thus, σ type aromaticity is expressed by NICS_{zz} in the center of the plane [NICS_{zz}(0)], while π , δ , and ϕ type aromaticities are expressed by NICS_{zz} 1 Å above the center of the plane [NICS_{zz}(1)].

Note that the NICS_{zz} scan curve given in Figure 8 was calculated for the structure obtained from the X-ray structural analysis of this system. The NICS_{zz}(1) (Bq located 1 Å above the {Hf₃} core) is equal to -44.6 ppm indicative of aromaticity. The magnetic aromaticity of the {Hf₃} core is comparable to that of benzene for which the NICS_{zz}(1) is calculated to be equal to -29.9 ppm at the GIAO/PBE0/6-31G(d,p) level. Also, the {Hf₃} core is more aromatic compared to a similar system bearing a {Zr₃} core and exhibiting NICS_{zz}(1) equal to -37.3 ppm.⁴⁰ However, the

presence of the O ligand capping the {Hf₃} ring contributes to the NICS_{zz}(1) values and so the aromaticity of the ring should be smaller. In this context, we used the NICS_{zz}(0) values to quantify the aromaticity of the three-member ring {Hf₃}. Accordingly, NICS_{zz}(0) is equal to -62.7 ppm suggesting strong σ -type metalloaromaticity of the {Hf₃} ring core. Interestingly, the {Hf₃} ring core exhibits a stronger metalloaromaticity than the respective {Zr₃} ring core with a NICS_{zz}(0) value equal to -40.1 ppm at the same level of theory.³⁶ The smaller size of the {Hf₃} ring relative to {Zr₃} ring accounts well for the observed higher metalloaromaticity of the former (the ring radius of the {Hf₃} ring is 1.996 Å as compared to the ring radius of 2.002 Å in the {Zr₃}). The perusal of Figure 8 reveals that the NICS_{zz} curve indicates the existence of multiple and alternating aromaticity/antiaromaticity zones. Away from the *cyclo*-{Hf₃} metallic cores, at distances of 2–3 Å from the metallic ring centers, there are two antiaromatic zones with NICS_{zz}(*R*) peak values around 32 ppm (at 2 Å below the ring plane) and around 18.1 ppm (at 2.6 Å above the ring plane). In contrast, at 0.5 near the O capping ligand (which is located 0.488 Å above the ring plane) the NICS_{zz}(1) is extremely high with a value equal to -107.3 ppm.

Photophysical Properties of HfOCs 1 and 3. Taking into consideration the interesting electronic structure and decreased band gap values observed above, we embarked on exploring the luminescence properties of the H₃dihybo and HfOCs 1 and 3 that are shown below in Table 5. The imide-

Table 5. Luminescence Data of H₃dihybo and the HfOCs 1 and 3 in Solution (MeOH, 1.00 mM)

compound	excitation (nm)	emission (nm)	quantum yield
H ₃ dihybo	362	417	42
H ₃ dihybo + 4 equiv of Et ₃ N	305	420	8
1	362	455	87
3	405	506	35

dioxime organic molecule H₃pidiox (Scheme 1) does not show any significant light emission. However, the pentanuclear HfOC 1 emits light at 455 nm upon excitation at 362 nm (Figure 9A). The excitation spectrum of HfOC 1 exhibits two excitation peaks at 362 and 400 nm. Cluster 1 has a low absorption of up to 500 nm (Figure S6). The intensity of the excitation peaks might be due to the energy transfer from the higher energy transitions of 1.⁸⁶

The catecholate–oxime organic molecule H₃dihybo (Scheme 1), emits light at 417 nm (Table 5) upon excitation at 362 nm.

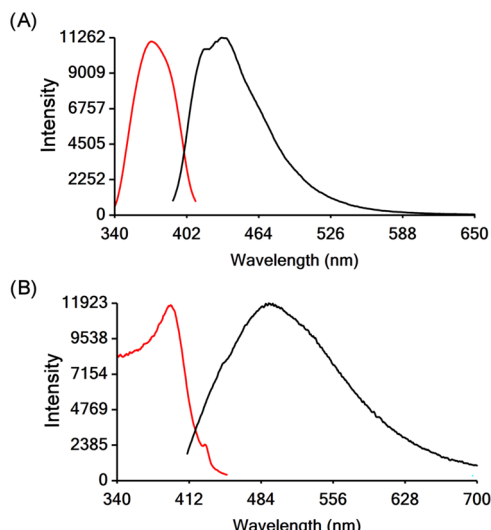


Figure 9. Excitation (red line) and emission (black line) spectra of (A) 1 and (B) 3 in solution (MeOH, 1.00 mM).

Upon complexation of the H₃dihybo ligand to the Hf(IV) centers in the hexanuclear HfOC 3, both the excitation and emission maximum wavelengths are shifted to lower energy, by 60 and 100 nm, respectively (Figure 9B and Table 5). HfOC 3 emits light in the cyan-green region (505 nm). The theoretical investigation of the luminescence properties of 1 and 3 (vide infra) predicts that the emitted light of these HfOCs is due to ligand–ligand electron transitions. However, ligation of the ligands to the Hf^{IV} centers results in a significant change in intensity and the wavelength of the emitted light. Considering that both ligands are strong chelators for hard metals, these ligands can be used for the extraction of Hf^{IV} by chelation and the above luminescence properties can be employed for sensing Hf^{IV} ions in solutions.

In an effort to further explore the emission behavior of clusters 1 and 3, we investigated the decay time of the excited state. In the case of compound 1 (Figure 10), the detection wavelength selected using the monochromator was 455 nm and the acquisition time was approximately 12 h to ensure a

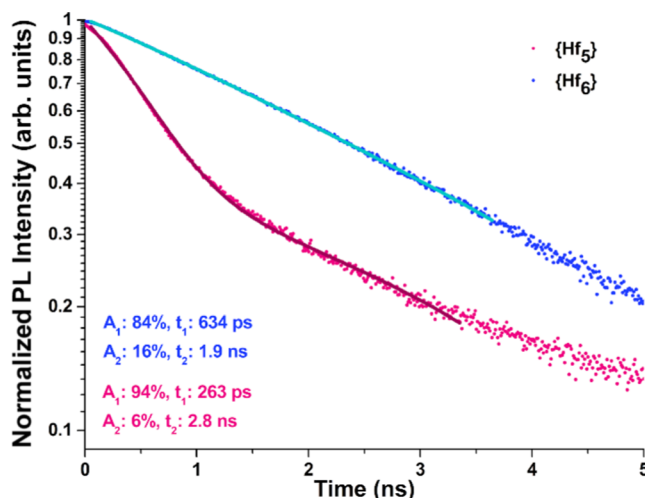


Figure 10. Photoluminescence decays of {Hf₆} 3 (upper, blue) and {Hf₅} 1 (lower, pink), shown with bi-exponential fits (solid lines) with parameters detailed in the inset and described in the main text.

good signal-to-noise ratio as shown. The lifetime exhibits a bi-exponential decay, where the fast component dominates significantly (~95%) at around 260 ps. The slow component makes up only 5% and is significantly slower, with a lifetime of just under 3 ns.

In the case of compound 3 (Figure 10), the detection wavelength was selected instead to be 520 nm and the acquisition time was as little as 3 h as it was slightly more emissive than the first sample. This ensured a similar signal-to-noise ratio to compound 1. The lifetime of the hexanuclear cluster 3 also exhibits a bi-exponential decay, where the fast component also dominates (~85%) but instead with a much slower lifetime of approximately 630 ps. Its slow component makes up only ~15% and is instead a whole nanosecond faster than that of the previous samples' slow decay component, with a lifetime of just under 2 ns.

Theoretical Study of the Optical Properties of HfOCs 1 {Hf₅} and 3 {Hf₆}. To tap into the optical properties of both complexes full geometry optimization of their single crystal coordinates was performed. The electronic structure of the ground states is typical of high-valent oxo complexes. The highest occupied molecular orbital–lowest unoccupied molecular orbital (HOMO–LUMO) gaps in {Hf₅} 1 and {Hf₆} 3 clusters are thus 2.68 and 2.29 eV (see Figures S12 and S13), respectively, showing a large separation between the oxo and metal “bands”. The value of 2.29 eV is very close to that of the experimental value of 2.36 eV from the UV–vis reflectance spectrum of the {Hf₆} 3 (vide supra).

The absorption spectrum of both systems was calculated at the time-dependent DFT (TD-revPBE-D4/TZP) level. It may be seen that for {Hf₆} 3 (Figure 11) the absorption wavelengths have excellent agreement with the experimental values although the absorption intensities are reversed. This may be an indication that in solution there may be a strong interaction with the solvent possibly through hydrogen bonds which cannot be captured by the implicit solvation scheme, and this leads consequently to symmetry breaking.

For {Hf₅} 1 (Figure 12) the agreement is not so good, and the bands are uniformly UV-shifted by 20–30 nm and their relative intensities are also reversed. Again, this may indicate relaxation effects and strong interaction with the solvent, inaccuracies in the level of theory, or the presence of protonation equilibria on the part of the hydroxo groups.

As the excitation source of the experiment is 405 nm this coincides with the first major band in {Hf₆} and the second one in {Hf₅}. As such the corresponding excited states that originate from those regions of the spectrum were optimized also by the TD-revPBE-D4 methodology.

In the case of {Hf₆}, the geometries of both the ground and excited states were optimized in global C₂ symmetry meaning that these will have A and B irreducible representations. Its absorption maximum (405 nm) corresponds to the 24th excited states in either symmetry representation, herein labeled as 24(¹A) and 24(¹B) and these are strictly degenerate in the ground state geometry. These electronic transitions are ascribed to the molecular orbitals that are mostly centered on the ligand. For this case, it was decided to pursue the relaxation of the 24(¹A) state.

In the case of {Hf₅}, the 20(¹A) and 20(¹B) states are not strictly degenerate but are still symmetry-related counterparts and are the origin of the first band maximum in the absorption region of 400 nm. The 20(¹A) root was therefore optimized.

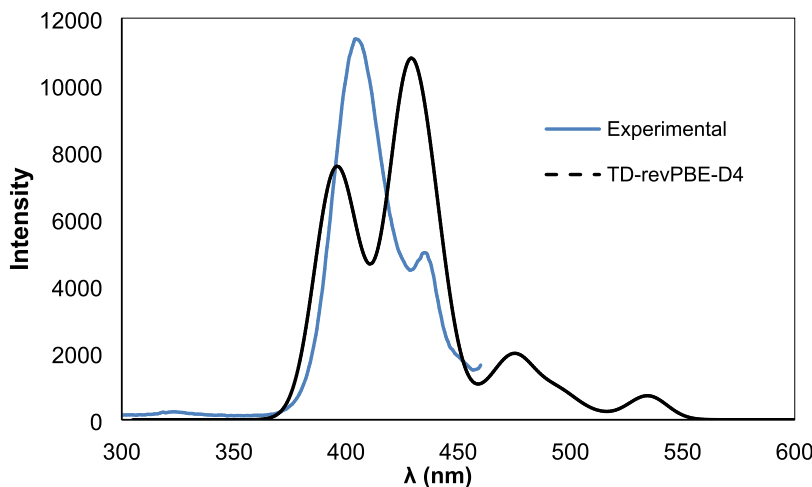


Figure 11. Excitation spectrum of HfOC 3 {Hf₆} contrasted with the calculated one.

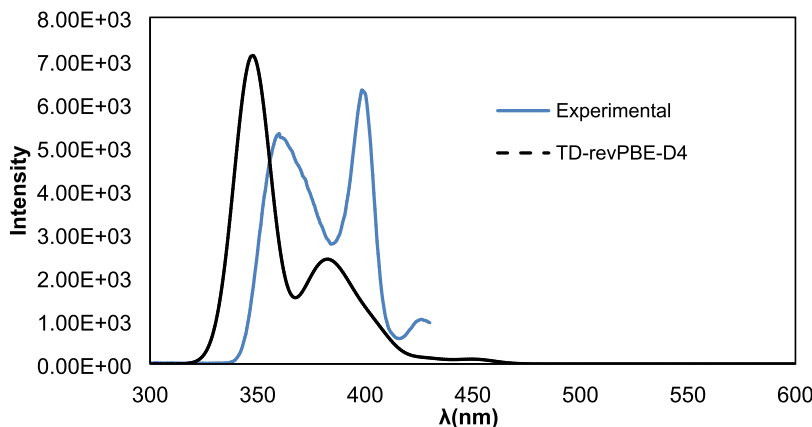


Figure 12. Excitation spectrum of HfOC 1 {Hf₅} contrasted with the calculated one.

In both {Hf₅} and {Hf₆} the targeted excited states have a ligand-to-ligand charge transfer (LLCT) character. The essential parameters are summarized in Table 6.

Table 6. Calculated Optical Parameters for HfOCs 1 {Hf₅} and 3 {Hf₆}

	{Hf ₆ }	{Hf ₅ }
state index	24(¹ A)	20(¹ A)
oscillator strength f_{OSC}	0.0144	0.0435
Franck–Condon (vertical) λ (nm)	404	388
emissive λ (nm)	515 (exp. 506)	443 (exp. 455)
adiabatic $\Delta E = E_{\text{ES}} - E_{\text{GS}}$ (eV)	2.801	2.799
radiative lifetime τ (s)	6.21×10^{-5}	5.36×10^{-6}
composition	42% NTO1 → NTO2	63% NTO1 → NTO2
	25% NTO3 → NTO4	22% NTO3 → NTO4

The transition density of {Hf₆} reflects the transition to and from the ligands' π orbital manifold (Figure 13). The associated natural transition orbitals for state 24(¹A) reflect a multi-configurational character with the majority of the transition being NTO1 → NTO2 (Table 6) while the second largest contribution stems from the NTO3 → NTO4 transition (Figure S14).

In the case of {Hf₅}, the transitions also exhibit an LLCT character (Figure 14) yet with a slightly more subtle metal 5d orbital involvement. The overwhelming contributions of the 20(¹A) state stem from NTO1 → NTO2 (Table 6) with a smaller contribution from NTO3 → NTO4 (Figure S15). Both calculated emission wavelengths (515 and 443 nm) are in good agreement with the experimentally determined maxima (506 and 455, respectively).

CONCLUSIONS

In summary, we have synthesized and characterized physicochemically a series of HfOCs with oxime ligands following a simple one-pot three-component reaction at room temperature. The flexible imide/dioxime ligand H₃pidiox stabilized a unique pentanuclear {Hf₅} structure 1, while the flat catecholate/oxime ligand H₃dihybo stabilized a hexanuclear {Hf₆} structure. The {Hf₅} cluster constitutes the first example of a pentanuclear hafnium(IV) cluster reported to date. The three {Hf₆} clusters (2–4) exhibit the same core structure [Hf₆^{IV}(μ_3 -O)₂(μ_2 -O)₃] with a trigonal-prismatic arrangement of the six hafnium atoms. Both the core structure and the trigonal-prismatic arrangement of the six hafnium atoms are unique.

The NICS_{zz} scan curves of the {Hf₆} system reveal the pronounced metalloaromaticity of the metallic {Hf₃} ring core. The calculated NICS_{zz}(1) value of -44.6 ppm is higher than that of -37.3 ppm for benzene and its {Zr₃} ring core analogue

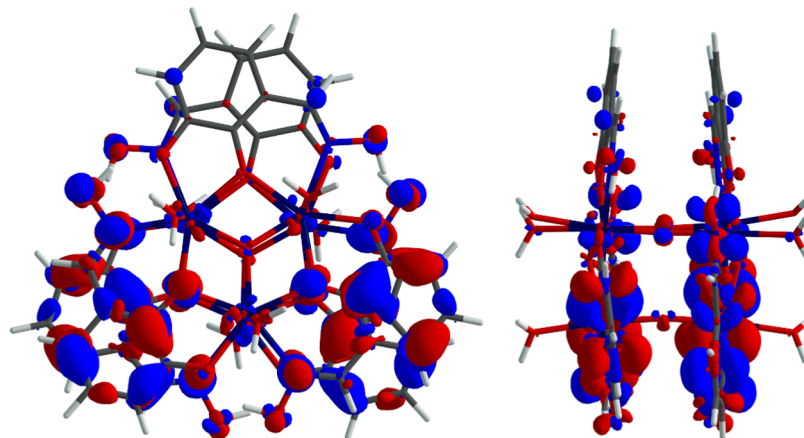


Figure 13. Top and side views of the calculated transition density of the emissive state of $\{ \text{Hf}_6 \}$. Blue regions represent electron depletion and red regions electron gain.

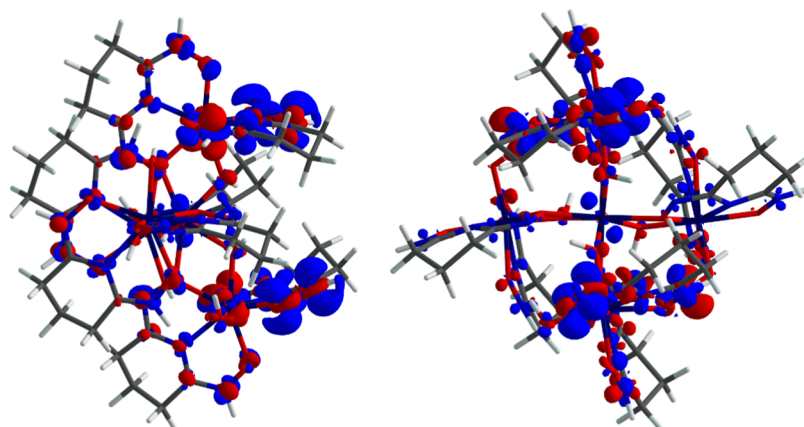


Figure 14. Two profile views of the calculated transition density of the emissive state of $\{ \text{Hf}_5 \}$. Blue regions represent electron depletion and red regions electron gain.

at the same level of theory. The ligation of the catechol oxime ligands to the Hf^{IV} ions, which are in a delocalized co-planar mode, gave rise to a remarkable reduction of the $\{ \text{Hf}_6 \}$ clusters' band gap in comparison to HfO_2 . X-ray diffraction studies and 2D $\{^1\text{H}\}$ NOESY NMR spectra revealed that the ligands of the two planes defined from each of the two $\{ \text{Hf}_3 \}$ cores are at a short distance and interact with each other through π -bonds enhancing further the reduction of the observed band gap. In addition, the pentanuclear and hexanuclear clusters formed by the ligation of the H_3pidiox and H_3dihybo to Hf^{IV} result in either emergence (in the case of 1) or substantial shifting the ligand's light emission (in the case of 1–3). Theoretical studies revealed that the origin of the luminescence properties observed in $\{ \text{Hf}_5 \}$ and $\{ \text{Hf}_6 \}$ HfOCs are due to intra-ligand electron transitions. There is a good agreement between the calculated and the experimentally determined emission band maxima. The difference in luminescence activity between the HfOCs and the free ligands might be attributed to the structural features of the former, in which the π orbital manifold of the organic ligands become polarized by their spatial arrangement in the molecules. These findings hint at an alternative strategy to develop new molecule-based materials that are photoactive in the visible region of the electromagnetic spectrum, by employing ligands that are only photoactive with UV light. Furthermore, NMR and ESI-MS studies in solution revealed that the reported HfOCs are thermodynamically

stable. The strong chelation of the catecholate–oxime ligand H_3dihybo to Hf^{IV} , and the remarkable aromaticity of the Hf_3^{IV} rings induce additional stability to the hexanuclear $\text{Hf}^{\text{IV}}/\text{H}_3\text{dihybo}$ HfOCs. The facile synthesis, thermodynamic stability, and the unique electronic structure that induces unique properties (aromaticity, fluorescence, low band gap values) to the hexanuclear $\text{Hf}^{\text{IV}}/\text{H}_3\text{dihybo}$ HfOCs render them highly promising candidates for the design of novel molecule-based materials with potential applications in chemistry and materials science, such as catalysis, molecular electronic devices, and sensing devices for hafnium. Development of hafnium sensing devices and optoelectronics is currently underway.

■ ASSOCIATED CONTENT

Data Availability Statement

The datasets for the stationary points obtained for the ground and excited state geometries are uploaded in the iochem-bd⁸⁷ database and accessible free of charge via <https://doi.org/10.19061/iochem-bd-6-147>.

● Supporting Information

The Supporting Information is available free of charge at <https://pubs.acs.org/doi/10.1021/acs.inorgchem.2c01768>.

UV–vis–near-infrared (NIR), Fourier transform infrared (FT-IR), NMR spectra, and crystallographic data ([PDF](#))

Accession Codes

CCDC 2172158–2172160 contain the supplementary crystallographic data for this paper. These data can be obtained free of charge via www.ccdc.cam.ac.uk/data_request/cif, or by emailing data_request@ccdc.cam.ac.uk, or by contacting The Cambridge Crystallographic Data Centre, 12 Union Road, Cambridge CB2 1EZ, UK; fax: +44 1223 336033.

■ AUTHOR INFORMATION

Corresponding Authors

Nuno A. G. Bandeira — *BioISI—BioSystems and Integrative Sciences Institute, Faculdade de Ciências da Universidade de Lisboa, 1749-016 Lisboa, Portugal;*  orcid.org/0000-0002-5754-7328; Email: nuno.bandeira@ciencias.ulisboa.pt

Athanassios C. Tsipis — *Section of Inorganic and Analytical Chemistry, University of Ioannina, Ioannina 45110, Greece;*  orcid.org/0000-0002-0425-2235; Email: attsipis@uoi.gr

Haralampos N. Miras — *WestCHEM, School of Chemistry, University of Glasgow, Glasgow G12 8QQ, U.K.;*  orcid.org/0000-0002-0086-5173; Email: charalampos.moiras@glasgow.ac.uk

Anastasios D. Keramidas — *Department of Chemistry, University of Cyprus, Nicosia 1678, Cyprus;*  orcid.org/0000-0002-0446-8220; Email: akeramid@ucy.ac.cy

Themistoklis A. Kabanos — *Section of Inorganic and Analytical Chemistry, University of Ioannina, Ioannina 45110, Greece;*  orcid.org/0000-0003-0357-2138; Email: tkampano@uoi.gr

Authors

Stamatis S. Passadis — *Section of Inorganic and Analytical Chemistry, University of Ioannina, Ioannina 45110, Greece*

Sofia Hadjithoma — *Department of Chemistry, University of Cyprus, Nicosia 1678, Cyprus*

Nicola J. Fairbairn — *WestCHEM, School of Chemistry, University of Glasgow, Glasgow G12 8QQ, U.K.;*  orcid.org/0000-0003-3984-7340

Gordon J. Hedley — *WestCHEM, School of Chemistry, University of Glasgow, Glasgow G12 8QQ, U.K.;*  orcid.org/0000-0002-1825-6296

Complete contact information is available at:

<https://pubs.acs.org/10.1021/acs.inorgchem.2c01768>

Author Contributions

Conceptualization, T.A.K., A.D.K. and H.N.M.; synthesis of the ligands and the hafnium(IV) compounds, S.S.P.; solid-state and solution UV-vis spectroscopy, S.S.P.; ESI-MS spectrometry H.N.M.; crystallography, H.N.M.; NMR spectroscopy, S.H. and A.D.K.; DFT calculations tackling spectroscopic properties, N.A.G.B.; time resolved spectroscopy, N.J.F. and G.J.H.; calculations related with aromaticity, A.C.T.; writing—original draft preparation, T.A.K., H.N.M., A.D.K., and S.S.P.; writing—review and editing, T.A.K., H.N.M., N.A.G.B. and A.D.K.; supervision of all contributions, T.A.K., H.N.M. and A.D.K. All authors have read and agreed to the published version of the manuscript.

Notes

The authors declare no competing financial interest.

■ ACKNOWLEDGMENTS

The research work was supported by the Hellenic Foundation for Research and Innovation (HFRI) under an HFRI Ph.D. Fellowship grant (Fellowship Number 1553) was funded by the European Regional Development Fund and the Republic of Cyprus through the Research and Innovation Foundation (Project: EXCELLENCE/1216/0515). H.N.M. thanks the University of Glasgow for supporting this work and Prof. L. Cronin for providing access to the X-ray and ESI-MS facilities. N.A.G.B. thanks Fundação para a Ciência e Tecnologia (grants PTDC/QUI-QFI/29236/2017, PTDC/QUI-QIN/0252/2021) and BioISI (UIDB-UIDP/04046/2020) for financial support. NAGB gratefully acknowledges the Institute of Chemical Research of Catalonia (ICIQ) and Prof. Carles Bo for allowing generous use of the “Kimik2” computational facilities.

■ REFERENCES

- (1) Gao, M. Y.; Chen, S.; Hu, L. X.; Zhang, L.; Zhang, J. Synthesis and photocatalytic H₂ evolution properties of four titanium-oxo clusters based on a cyclohex-3-ene-1-carboxylate ligand. *Dalton Trans.* **2017**, *46*, 10630–10634.
- (2) Hou, J.-L.; Huo, P.; Tang, Z.-Z.; Cui, L.-N.; Zhu, Q.-Y.; Dai, J. A Titanium Oxo Cluster Model Study of Synergistic Effect of Coordinated Dye Ligands on Photocurrent Responses. *Inorg. Chem.* **2018**, *57*, 7420–7427.
- (3) Wang, C.; Liu, C.; Li, L. J.; Sun, Z. M. Synthesis, Crystal Structures, and Photochemical Properties of a Family of Heterometallic Titanium Oxo Clusters. *Inorg. Chem.* **2019**, *58*, 6312–6319.
- (4) Xu, T.; Hou, X.; Wang, Y.; Zhang, J.; Zhang, J.; Liu, B. A gigantic polyoxozirconate with visible photoactivity. *Dalton Trans.* **2017**, *46*, 10185–10188.
- (5) Zou, D.-H.; Cui, L.-N.; Liu, P.-Y.; Yang, S.; Zhu, Q.-Y.; Dai, J. Molecular Model of Dye Sensitized Titanium Oxides Based on Arylamine Dye Anchored Titanium Oxo Clusters. *Inorg. Chem.* **2019**, *58*, 9246–9252.
- (6) Janek, M.; Muzioł, T. M.; Piszczełk, P. Trinuclear Oxo-Titanium Clusters: Synthesis, Structure, and Photocatalytic Activity. *Materials* **2019**, *12*, No. 3195.
- (7) Janek, M.; Radtke, A.; Muzioł, T. M.; Jerzykiewicz, M.; Piszczełk, P. Tetranuclear Oxo-Titanium Clusters with Different Carboxylate Aromatic Ligands: Optical Properties, DFT Calculations, and Photoactivity. *Materials* **2018**, *11*, No. 1661.
- (8) Passadis, S. S.; Hadjithoma, S.; Siafarika, P.; Kalampounias, A. G.; Keramidas, A. D.; Miras, H. N.; Kabanos, T. A. Synthesis, Structural and Physicochemical Characterization of a Titanium(IV) Compound with the Hydroxamate Ligand N,2-Dihydroxybenzamide. *Molecules* **2021**, *26*, No. 5588.
- (9) Zhang, Y.; Azambuja, F.; Parac-Vogt, T. N. The forgotten chemistry of group(IV) metals: A survey on the synthesis, structure, and properties of discrete Zr(IV), Hf(IV), and Ti(IV) oxo clusters. *Coord. Chem. Rev.* **2021**, *438*, No. 213886.
- (10) Sommers, J. A.; Palys, L.; Martin, N. P.; Fast, D. B.; Amiri, M.; Nyman, M. Oxo-Cluster-Based Zr/HfIV Separation: Shedding Light on a 70-Year-Old Process. *J. Am. Chem. Soc.* **2022**, *144*, 2816–2824.
- (11) Kozma, K.; Zakharov, L. N.; Nyman, M. Counterion-Controlled Nuclearity of Zr/Hf Peroxo Oxalates. *Cryst. Growth Des.* **2020**, *20*, 6519–6527.
- (12) Sommers, J. A.; Hutchison, D. C.; Martin, N. P.; Kozma, K.; Keszler, D. A.; Nyman, M. Peroxide-Promoted Disassembly Reassembly of Zr-Polyoxocation. *J. Am. Chem. Soc.* **2019**, *141*, 16894–16902.
- (13) Sommers, J. A.; Hutchison, D. C.; Martin, N. P.; Palys, L.; Amador, J. M.; Keszler, D. A.; Nyman, M. Differentiating Zr/HfIV Aqueous Polyoxocation Chemistry with Peroxide Ligation. *Inorg. Chem.* **2021**, *60*, 1631–1640.

- (14) Frederick, R. T.; Amador, J. M.; Goberna-Ferron, S.; Nyman, M.; Keszler, D. A.; Herman, G. S. Mechanistic Study of HafSO_x Extreme Ultraviolet Inorganic Resists. *J. Phys. Chem. C* **2018**, *122*, 16100–16112.
- (15) Anderson, J. T.; Munsee, C. L.; Hung, C. M.; Phung, T. M.; Herman, G. S.; Johnson, D. C.; Wager, J. F.; Keszler, D. A. Solution-Processed HafSO_x and ZircSO_x Inorganic Thin-Film Dielectrics and Nanolaminates. *Adv. Funct. Mater.* **2007**, *17*, 2117–2124.
- (16) Stowers, J.; Keszler, D. A. High resolution, high sensitivity inorganic resists. *Microelectron. Eng.* **2009**, *86*, 730–733.
- (17) Moons, J.; Azambuja, F.; Mihailovic, J.; Kozma, K.; Smiljanic, K.; Amiri, M.; Cirkovic-Velickovic, T.; Nyman, M.; Parac-Vogt, T. N. Discrete Hf18 metal-oxo cluster as a heterogeneous nanzyme for site-specific proteolysis. *Angew. Chem., Int. Ed.* **2020**, *59*, 9094–9101.
- (18) Hu, Z.; Nalaparaju, A.; Peng, Y.; Jiang, J.; Zhao, D. Modulated Hydrothermal Synthesis of UiO-66(Hf)-Type Metal-Organic Frameworks for Optimal Carbon Dioxide Separation. *Inorg. Chem.* **2016**, *55*, 1134–1141.
- (19) Hu, Z.; Castano, I.; Wang, S.; Wang, Y.; Peng, Y.; Qian, Y.; Chi, C.; Wang, X.; Zhao, D. Modulator Effects on the Water-Based Synthesis of Zr/Hf Metal-Organic Frameworks: Quantitative Relationship Studies between Modulator, Synthetic Condition, and Performance. *Cryst. Growth Des.* **2016**, *16*, 2295–2301.
- (20) Xydias, P.; Spanopoulos, I.; Klontzas, E.; Froudakis, G. E.; Trikalitis, P. N. Drastic Enhancement of the CO₂ Adsorption Properties in Sulfone-Functionalized Zr- and Hf-UiO-67 MOFs with Hierarchical Mesopores. *Inorg. Chem.* **2014**, *53*, 679–681.
- (21) Rojas-Buzo, S.; García-García, P.; Corma, A. Hf-based Metal-Organic Frameworks as acid-base catalysts for the transformation of biomass-derived furanic compounds into chemicals. *Green Chem.* **2018**, *20*, 3081–3091.
- (22) Bakuru, V. R.; Davisa, D.; Kalidindi, S. B. Cooperative catalysis at the metal–MOF interface: hydrodeoxygenation of vanillin over Pd nanoparticles covered with a UiO-66(Hf) MOF. *Dalton Trans.* **2019**, *48*, 8573.
- (23) Otake, K.-i.; Ye, J.; Mandal, M.; Islamoglu, T.; Buru, C. T.; Hupp, J. T.; Delferro, M.; Truhlar, D. G.; Cramer, C. J.; Farha, O. Enhanced Activity of Heterogeneous Pd(II) Catalysts on Acid-Functionalized Metal–Organic Frameworks. *ACS Catal.* **2019**, *9*, 5383–5390.
- (24) Rojas-Buzo, S.; García-García, P.; Corma, A. Catalytic Transfer Hydrogenation of Biomass-Derived Carbonyls over Hafnium-Based Metal-Organic Frameworks. *ChemSusChem* **2018**, *11*, 432–438.
- (25) Du, X. D.; Yi, X. H.; Wang, P.; Zheng, W.; Deng, J.; Wang, C. C. Robust Photocatalytic Reduction of Cr(VI) on UiO-66-NH₂ (Zr/Hf) Metal-Organic Framework Membrane under Sunlight Irradiation. *Chem. Eng. J.* **2019**, *356*, 393–399.
- (26) Das, A.; Anubub, N.; Dhakshinamoorthy, A.; Biswas, S. A highly catalytically active Hf(IV) metal-organic framework for Knoevenagel condensation. *Microporous Mesoporous Mater.* **2019**, *284*, 459–467.
- (27) Nguyen, L. H. T.; Nguyen, T. T.; Nguyen, H. L.; Doan, T. L. H.; Tran, P. H. A new superacid hafnium-based metal-organic framework as a highly active heterogeneous catalyst for the synthesis of benzoxazoles under solvent-free condition. *Catal. Sci. Technol.* **2017**, *7*, 4346–4350.
- (28) Rimoldi, M.; Howarth, A. J.; DeStefano, M. R.; Lin, L.; Goswami, S.; Li, P.; Hupp, J. T.; Farha, O. K. Catalytic zirconium/hafnium-based Metal–Organic frameworks. *ACS Catal.* **2017**, *7*, 997–1014.
- (29) Lustig, W. P.; Mukherjee, S.; Rudd, N. D.; Desai, A. V.; Li, J.; Ghosh, S. K. Metal–organic frameworks: functional luminescent and photonic materials for sensing applications. *Chem. Soc. Rev.* **2017**, *46*, 3242–3285.
- (30) Jakobsen, S.; Gianolio, D.; Wragg, D. S.; Nilsen, M. H.; Emerich, H.; Bordiga, S.; Lamberti, C.; Olsbye, U.; Tilset, M.; Lillerud, K. P. Structural Determination of a Highly Stable MetalOrganic Framework with Possible Application to Interim Radioactive Waste Scavenging: Hf-UiO-66. *Phys. Rev. B: Condens. Matter Mater. Phys.* **2012**, *86*, No. 125429.
- (31) Buckley, J. D. *Stabilization of the Phase Transformations in Hafnium Oxide*; Iowa State University, 1968.
- (32) Lee, S. J.; Jeon, T. S.; Kwong, D. L.; Clark, R. Hafnium oxide gate stack prepared by in situ rapid thermal chemical vapor deposition process for advanced gate dielectrics. *J. Appl. Phys.* **2002**, *92*, 2807.
- (33) Xu, Z.; Houssa, M.; Gendt, S. D.; Heyns, M. Polarity effect on the temperature dependence of leakage current through HfO₂/SiO₂ gate dielectric stacks. *Appl. Phys. Lett.* **2002**, *80*, 1975.
- (34) Yu, S.; Guan, X.; Wong, H.-S. P. Conduction mechanism of TiN/HfO_x/Pt resistive switching memory: A trapassisted-tunneling model. *Appl. Phys. Lett.* **2011**, *99*, No. 063507.
- (35) Mueller, S.; Mueller, J.; Singh, A.; Riedel, S.; Sundqvist, J.; Schroeder, U.; Mikolajick, T. Incipient Ferroelectricity in Al-Doped HfO₂ Thin Films. *Adv. Funct. Mater.* **2012**, *22*, 2412–2417.
- (36) Martin, D.; Yurchuk, E.; Müller, S.; Müller, J.; Paul, J.; Sundquist, J.; Slesazeck, S.; Schlosser, T.; Bentum, R.; Trentzsch, M.; Schröder, U.; Mikolajick, T. Downscaling ferroelectric field effect transistors by using ferroelectric Si-doped HfO₂. *Solid-State Electron.* **2013**, *88*, 65–68.
- (37) Müller, J.; Schroder, U.; Boscke, T. S.; Muller, I.; Bottger, U.; Wilde, L.; Sundqvist, J.; Lemberger, M.; Kucher, P.; Mikolajick, T.; Frey, L. Ferroelectricity in yttrium-doped hafnium oxide. *J. Appl. Phys.* **2011**, *110*, No. 114113.
- (38) Hintersehr, J. Process for Producing Dental Prostheses. US5,702,650A, 1997. <http://www.google.com/patents/US5702650>.
- (39) Suvorova, E. I.; Uvarov, O. V.; Arkharova, N. A.; Ibrayeva, A. D.; Skuratov, V. A.; Buffat, P. A. Structure evolution, bandgap, and dielectric function in La-doped hafnium oxide thin layer subjected to swift Xe ion irradiation. *J. Appl. Phys.* **2020**, *128*, No. 164103. and references therein.
- (40) Passadis, S. S.; Papanikolaou, M. G.; Elliott, A.; Tsiafoulis, C. G.; Tsipis, A. C.; Keramidas, A. D.; Miras, H. N.; Kabanos, T. A. Synthesis, Structural, and Physicochemical Characterization of a Ti₆ and a Unique Type of Zr₆ Oxo Clusters Bearing an Electron-Rich Unsymmetrical {OON} Catecholate/Oxime Ligand and Exhibiting Metalloaromaticity. *Inorg. Chem.* **2020**, *59*, 18345–18357.
- (41) Lv, H. T.; Li, H. M.; Zou, G. D.; Cui, Y.; Huang, Y.; Fan, Y. Titanium-oxo clusters functionalized with catecholate-type ligands: modulating the optical properties through charge transfer transitions. *Dalton Trans.* **2018**, *47*, 8158–8163.
- (42) Yu, Y.-Z.; Zhang, Y.-R.; Geng, C.-H.; Sun, L.; Guo, Y.; Feng, Y.-R.; Wang, Y.-X.; Zhang, X.-M. Precise and Wide-Ranged Band-Gap Tuning of Ti₆-Core-Based Titanium Oxo Clusters by the Type and Number of Chromophore Ligands. *Inorg. Chem.* **2019**, *58*, 16785–16791.
- (43) Passadis, S. S.; Hadjithoma, S.; Kalampounias, A. G.; Tsipis, A. C.; Sproules, S.; Miras, H. N.; Keramidas, A. D.; Kabanos, T. A. Synthesis, structural and physicochemical characterization of a new typeTi₆-oxo cluster protected by a cyclic imide dioxime ligand. *Dalton Trans.* **2019**, *48*, 5551–5559.
- (44) Passadis, S. S.; Hadjithoma, S.; Papanikolaou, M. G.; Keramidas, A. D.; Miras, H. N.; Kabanos, T. A. Acid/base responsive assembly/dis-assembly of a family of zirconium(IV) clusters with a cyclic imide-dioxime ligand. *Dalton Trans.* **2022**, *51*, 1806–1818.
- (45) (a) Assi, H.; Haouas, M.; Mouchaham, G.; Martineau-Corcos, C.; Allain, C.; Clavier, G.; Guillou, N.; Serre, C.; Devic, T. MgTi(cat)3, a promising precursor for the preparation of Ti-MOFs? *Polyhedron* **2018**, *156*, 111–115. (b) Cooper, S. R.; Koh, Y. B.; Raymond, K. N. Synthetic, Structural, and Physical Studies of Bis(triethylammonium) Tris(catecholato)vanadate(IV), Potassium Bis(catecholato)- oxovanadate(IV), and Potassium T ris-(catecholato)vanadate(III). *J. Am. Chem. Soc.* **1982**, *104*, 5092–5102. (c) Harris, W. R.; Carrano, C. J.; Cooper, S. R.; Sofen, S. R.; Avdeef, A. E.; McArdle, J. V.; Raymond, K. N. Coordination Chemistry of Microbial Iron Transport Compounds. 19. Stability Constants and Electrochemical Behavior of Ferric Enterobactin and Model Complexes. *J. Am. Chem. Soc.* **1979**, *101*, 6097. (d) Sofen, S.

- R.; Cooper, S. R.; Raymond, K. N. Crystal and Molecular Structures of Tetrakis(catecholato)hafnate(IV) and -cerate- (IV). Further Evidence for a Ligand Field Effect in the Structure of Tetrakis(catecholato)uranate(IV). *Inorg. Chem.* **1979**, *18*, 1611–1616.
- (e) Borgias, B. A.; Cooper, S. R.; Koh, Y. B.; Raymond, K. N. Synthetic, Structural, and Physical Studies of Titanium Complexes of Catechol and 3,5-Di- tert – butylcatechol. *Inorg. Chem.* **1984**, *23*, 1009–1016.
- (46) (a) Baumann, S. O.; Bendova, M.; Puchberger, M.; Schubert, U. Modification of Titanium Isopropoxide with Aromatic Aldoximes. *Eur. J. Inorg. Chem.* **2011**, *2011*, 573–580. (b) Baumann, S. O.; Puchberger, M.; Schubert, U. Oximate-substituted zirconium alkoxides. *Dalton Trans.* **2011**, *40*, 1401–1406.
- (47) Li, N.; Yang, L.; Wang, D.; Tang, C.; Deng, W.; Wang, Z. High-Capacity Amidoxime-Functionalized β -Cyclodextrin/Graphene Aerogel for Selective Uranium Capture. *Environ. Sci. Technol.* **2021**, *55*, 9181–9188.
- (48) Sun, Q.; Aguila, B.; Perman, J.; Ivanov, A. S.; Bryantsev, V. S.; Earl, L. D.; Abney, C. W.; Wojtas, L.; Ma, S. Bio-inspired nano-traps for uranium extraction from seawater and recovery from nuclear waste. *Nat. Commun.* **2018**, *9*, No. 1644.
- (49) Hadjithoma, S.; Papanikolaou, M. G.; Leontidis, E.; Kabanos, T. A.; Keramidas, A. D. Bis(hydroxylamino)triazines: High Selectivity and Hydrolytic Stability of Hydroxylamine-Based Ligands for Uranyl Compared to Vanadium(V) and Iron(III). *Inorg. Chem.* **2018**, *57*, 7631–7643.
- (50) Feixas, F.; Matito, E.; Jordi Poater, J.; Sola, M. Metaloaromaticity. *WIREs Comput. Mol. Sci.* **2013**, *3*, 105–122.
- (51) (a) Esteruelas, M. A.; Fernandez, I.; Cristina García-Yebra, C.; Martín, J.; Oñate, E. Cycloosmathioborane Compounds: Other Manifestations of the Hückel Aromaticity. *Inorg. Chem.* **2019**, *58*, 2265–2269. (b) Cook, A. W.; Hrobarik, P.; Damon, P. L.; Wu, G.; Hayton, T. W. A Ketimide-Stabilized Palladium Nanocluster with a Hexagonal Aromatic Pd₇ Core. *Inorg. Chem.* **2020**, *59*, 1471–1480. (c) Zhu, Q.; Chen, S.; Xu, F.; Zhu, I. Reaction Mechanisms on [3 + 2] Cycloaddition of Azides with Metal Carbyne Complexes: Significant Effects of Aromaticity, Substituent, and Metal Center. *Inorg. Chem.* **2020**, *59*, 7318–7324. (d) Cusumano, A. Q.; Goddard, W. A.; Stoltz, B. M. The Transition Metal Catalyzed [π 2s + π 2s + σ 2s + σ 2s] Pericyclic Reaction: Woodward–Hoffmann Rules, Aromaticity, and Electron Flow. *J. Am. Chem. Soc.* **2020**, *142*, 19033–19039. (e) Kopp, S. M.; Gotfredsen, H.; Deng, J. R.; Claridge, T. D. W.; Anderson, H. A. Global Aromaticity in a Partially Fused 8-Porphyrin Nanoring. *J. Am. Chem. Soc.* **2020**, *142*, 19393–19401. (f) Pagano, J. K.; Xie, J.; Erickson, K. A.; Cope, S. K.; Scott, B. L.; Wu, R.; Waterman, R.; Morris, D. E.; Yang, P.; Gagliardi, L.; Kiplinger, J. L. Actinide 2-metallabiphenylenes that satisfy Hückel's rule. *Nature* **2020**, *578*, 563–567. (g) Ueta, K.; Kim, J.; Ooi, S.; Oh, J.; Shin, J.; Nakai, A.; Lim, M.; Tanaka, T.; Kim, D.; Osuka, A. meso-Oxoisocorroles: Tunable Antiaromaticity by Metalation and Coordination of Lewis Acids as Well as Aromaticity Reversal in the Triplet Excited State. *J. Am. Chem. Soc.* **2021**, *143*, 7958–7967. (h) Kawashima, H.; Ukai, S.; Nozawa, R.; Fukui, N.; Fitzsimmons, G.; Kowalczyk, T.; Flieg, H.; Shinokubo, H. Determinant Factors of Three-Dimensional Aromaticity in Antiaromatic Cyclophanes. *J. Am. Chem. Soc.* **2021**, *143*, 10676–10685.
- (52) Chen, Z.-N.; Fu, G.; Zhang, I. Y.; Xu, X. Understanding the Nonplanarity in Aromatic Metallabenzenes: A σ -Control Mechanism. *Inorg. Chem.* **2018**, *57*, 9205–9214. and references therein.
- (53) Higino Damasceno, J.; Teixeira Rabelo, J. N.; Candido, L. Electron Correlation Effects in All-Metal Aromatic Clusters: A Quantum Monte Carlo Study. *Inorg. Chem.* **2016**, *55*, 7442–7447. and references therein.
- (54) (a) Tanaka, H.; Neukermans, S.; Janssens, E.; Silverans, R. E.; Lievens, P. σ Aromaticity of the Bimetallic Au₅Zn⁺ Cluster. *J. Am. Chem. Soc.* **2003**, *125*, 2862–2863. (b) Li, Y.; Oliveira, V.; Tang, C.; Cremer, D.; Liu, C.; Ma, J. The Peculiar Role of the Au₃ Unit in Aum Clusters: σ -Aromaticity of the Au₅Zn⁺ Ion. *Inorg. Chem.* **2017**, *56*, 5793–5803.
- (55) Iron, M. A.; Martin, J. M. L.; van der Boom, M. E. Cycloaddition Reactions of Metallocaromatic Complexes of Iridium and Rhodium: A Mechanistic DFT Investigation. *J. Am. Chem. Soc.* **2003**, *125*, 11702–11709.
- (56) Li, X.; Sun, J.; Zeng, Y.; Sun, Z.; Zheng, S.; Meng, L. Nature of Chemical Bonding and Metallocaromaticity of Na₂[MArx')₃] (M = B, Al, Ga; Arx' = C₆H₃-2,6-(C₆H₅)₂). *J. Phys. Chem. A* **2012**, *116*, 5491–5496.
- (57) Nembach, E. Order strengthening: recent developments, with special reference to aluminium±lithium-alloys. *Prog. Mater. Sci.* **2000**, *45*, 275–338.
- (58) Chen, Z.; Wannere, C. S.; Corminboeuf, C.; Puchta, R.; Schleyer, P.v.P. Nucleus-Independent Chemical Shifts (NICS) as an Aromaticity Criterion. *Chem. Rev.* **2005**, *105*, 3842–3888.
- (59) Cabello, G.; Lillo, L.; Buono-Core, G. E. Zr(IV) and Hf(IV) β -diketonate complexes as precursors for the photochemical deposition of ZrO₂ and HfO₂ thin films. *J. Non-Cryst. Solids* **2008**, *354*, 982–988.
- (60) Knör, G.; Strasser, A. Coexisting intraligand fluorescence and phosphorescence of hafnium(IV) and thorium(IV) porphyrin complexes in solution. *Inorg. Chem. Commun.* **2002**, *5*, 993.
- (61) Zhang, K. Y.; Lo, K. K. W. Chemosensing and Diagnostics. In *Comprehensive Inorganic Chemistry II: From Elements to Applications*, 2nd ed.; Elsevier Ltd., 2013; Vol. 8, pp 657–732.
- (62) Hudson, Z. M.; Wang, S. Metal-containing triarylboron compounds for optoelectronic applications. *Dalton Trans.* **2011**, *40*, 7805–7816.
- (63) Baerends, E. J.; Ziegler, T.; Atkins, A. J.; Autschbach, J.; Baseggio, O.; Bashford, D.; Bérces, A.; Bickelhaupt, F. M.; Bo, C.; Boerriger, P. M.; Cavallo, L.; Daul, C.; Chong, D. P.; Chulhai, D. V.; Deng, L.; Dickson, R. M.; Dieterich, J. M.; Ellis, D. E.; van Faassen, M.; Fan, L.; Fischer, T. H.; Fonseca Guerra, C.; Franchini, M.; Ghysels, A.; Giannoni, A.; van Gisbergen, S.J.A.; Goez, A.; Götz, A. W.; Groeneveld, J. A.; Gritsenko, O. V.; Grüning, M.; Gusarov, S.; Harris, F. E.; van den Hoek, P.; Hu, Z.; Jacob, C. R.; Jacobsen, H.; Jensen, L.; Joubert, L.; Kaminski, J. W.; van Kessel, G.; König, C.; Kootstra, F.; Kovalenko, A.; Krykunov, M. V.; van Lenthe, E.; McCormack, D. A.; Michalak, A.; Mitoraj, M.; Morton, S. M.; Neugebauer, J.; Nicu, V. P.; Noddleman, L.; Osinga, V. P.; Patchkovskii, S.; Pavanello, M.; Peeples, C. A.; Philipsen, P.H.T.; Post, D.; Pye, C. C.; Ramanantoanina, H.; Ramos, P.; Ravenek, W.; Rodriguez, J. I.; Ros, P.; Rüger, R.; Schipper, P.R.T.; Schlüns, D.; van Schoot, H.; Schreckenbach, G.; Seldenthuis, J. S.; Seth, M.; Snijders, J. G.; Solà, M.; Stener, M.; Swart, M.; Swerhone, D.; Tognetti, V.; te Velde, G.; Vernooyjs, P.; Versluis, L.; Visscher, L.; Visser, O.; Wang, F.; Wesolowski, T. A.; van Wezenbeek, E. M.; Wiesenecker, G.; Wolff, S. K.; Woo, T. K.; Yakovlev, A. L. *Scientific Computing and Modelling*, ADF-2019.304; SCM, 2019. <http://www.scm.com>.
- (64) Zhang, Y.; Yang, W. Comment on “Generalized Gradient Approximation Made Simple”. *Phys. Rev. Lett.* **1998**, *80*, 890.
- (65) Perdew, J. P.; Burke, K.; Ernzerhof, M. Generalized gradient approximation made simple. *Phys. Rev. Lett.* **1996**, *77*, 3865–3868.
- (66) Caldeweyher, E.; Bannwarth, C.; Grimme, S. Extension of the D₃ dispersion coefficient model. *J. Chem. Phys.* **2017**, *147*, No. 034112.
- (67) Klamt, A.; Schüürmann, G. COSMO: a new approach to dielectric screening in solvents with explicit expressions for the screening energy and its gradient. *J. Chem. Soc., Perkin Trans. 2* **1993**, 799–805.
- (68) (a) van Lenthe, E.; Baerends, E. J.; Snijders, J. G. Relativistic regular two-component Hamiltonians. *J. Chem. Phys.* **1993**, *99*, 4597–4610. (b) van Lenthe, E.; Ehlers, A. E.; Baerends, E. J. Geometry optimizations in the zero order regular approximation for relativistic effects. *J. Chem. Phys.* **1999**, *110*, 8943–8953.
- (69) Casida, M. E. Time-Dependent Density Functional Response Theory for Molecules. In *Recent Advances in Density Functional Methods*; Chong, D. P., Ed.; World Scientific, 1995; pp 155–192.
- (70) Ditchfield, R. Self-consistent perturbation theory of diamagnetism. *Mol. Phys.* **1974**, *27*, 789–807.

- (71) Gauss, J. Effects of electron correlation in the calculation of nuclear magnetic resonance chemical shifts. *J. Chem. Phys.* **1993**, *99*, 3629–3643.
- (72) Frisch, M. J.; Trucks, G. W.; Schlegel, H. B.; Scuseria, G. E.; Robb, M. A.; Cheeseman, J. R.; Scalmani, G.; Barone, V.; Mennucci, B.; Petersson, G. A.; Nakatsuji, H.; Caricato, M.; Li, X.; Hratchian, H. P.; Izmaylov, A. F.; Bloino, J.; Zheng, G.; Sonnenberg, J. L.; Hada, M.; Ehara, M.; Toyota, K.; Fukuda, R.; Hasegawa, J.; Ishida, M.; Nakajima, T.; Honda, Y.; Kitao, O.; Nakai, H.; Vreven, T.; Montgomery, J. A., Jr.; Peralta, J. E.; Ogliaro, F.; Bearpark, M.; Heyd, J. J.; Brothers, E.; Kudin, K. N.; Staroverov, V. N.; Kobayashi, R.; Normand, J.; Raghavachari, K.; Rendell, A.; Burant, J. C.; Iyengar, S. S.; Tomasi, J.; Cossi, M.; Rega, N.; Millam, N. J.; Klene, M.; Knox, J. E.; Cross, J. B.; Bakken, V.; Adamo, C.; Jaramillo, J.; Gomperts, R.; Stratmann, R. E.; Yazyev, O.; Austin, A. J.; Cammi, R.; Pomelli, C.; Ochterski, J. W.; Martin, R. L.; Morokuma, K.; Zakrzewski, V. G.; Voth, G. A.; Salvador, P.; Dannenberg, J. J.; Dapprich, S.; Daniels, A. D.; Farkas, Ö.; Foresman, J. B.; Ortiz, J. V.; Cioslowski, J.; Fox, D. J. *Gaussian 09*, revision C.01; Gaussian Inc., 2009.
- (73) Gross, S.; Kickelbick, G.; Puchberger, M.; Schubert, U. Mono-, Di-, and Trimetallic Methacrylate-substituted Metal Oxide Clusters Derived from Hafnium Butoxide. *Monatsh. Chem.* **2003**, *134*, 1053–1063.
- (74) Kalaji, A.; Soderholm, L. Aqueous Hafnium Sulfate Chemistry: Structures of Crystalline Precipitates. *Inorg. Chem.* **2014**, *53*, 11252.
- (75) Goberna-Ferrón, S.; Park, D.-H.; Amador, J. M.; Keszler, D. A.; Nyman, M. Amphoteric Aqueous Hafnium Cluster Chemistry. *Angew. Chem., Int. Ed.* **2016**, *55*, 6221–6224.
- (76) Boyle, T. J.; Tribby, L. J.; Alam, T. M.; Bunge, S. D.; Holland, G. P. Catechol derivatives of Group 4 and 5 compounds. *Polyhedron* **2005**, *24*, 1143–1152.
- (77) Braunwarth, W.; Thewalt, U. Polynuclear CpZr(IV) and CpHf(IV) Complexes with Oximate Bridges. *Z. Naturforsch. B* **1997**, *52*, 1011–1018.
- (78) Shi, C.; Zhang, M.; Hang, X.; Bi, Y.; Huang, L.; Zhou, K.; Xu, Z.; Zheng, Z. Assembly of thiocalix[4]arene-supported high-nucularity Cd24 cluster with enhanced photocatalytic activity. *Nanoscale* **2018**, *10*, 14448–14454.
- (79) (a) Miras, H. N.; Sorus, M.; Hawkett, J.; Sells, D. O.; McInnes, E. L.; Cronin, L. Oscillatory template exchange in polyoxometalate capsules: a ligand-triggered, redox-powered, chemically damped oscillation. *J. Am. Chem. Soc.* **2012**, *134*, 6980–6983. (b) Miras, H. N.; Wilson, E. F.; Cronin, L. Unravelling the complexities of inorganic and supramolecular self-assembly in solution with electrospray and cryospray mass spectrometry. *Chem. Commun.* **2009**, *11*, 1297–1311.
- (80) Miras, H. N.; Long, D. L.; Kögerler, P.; Cronin, L. Bridging the gap between solution and solid-state studies in polyoxometalate chemistry: Discovery of a family of [V1M17]-based cages encapsulating two {(VO₄)O-V} moieties. *Dalton Trans.* **2008**, *52*, 214–221.
- (81) (a) Zang, H. Y.; Chen, J. J.; Long, D. L.; Cronin, L.; Miras, H. N. Assembly of Thiometalate-Based {Mo16} and {Mo36} Composite Clusters Combining [Mo₂O₂S₂]²⁺ Cations and Selenite Anions. *Adv. Mater.* **2013**, *25*, 6245–6249. (b) Yan, J.; Long, D. L.; Miras, H. N.; Cronin, L. Cation controlled assembly and transformation of mono- and bi-sulfite templated Dawson-type polyoxotungstates. *Inorg. Chem.* **2010**, *49*, 1819–1825.
- (82) Schleyer, P. V. R.; Maerker, C.; Dransfeld, A.; Jiao, H.; van Eikema Hommes, N. J. R. Nucleus-independent chemical shifts: a simple and efficient aromaticity probe. *J. Am. Chem. Soc.* **1996**, *118*, 6317–6318.
- (83) Schleyer, P. V. R.; Manoharan, M.; Wang, Z. X.; Kiran, B.; Jiao, H.; Puchta, R.; Van Eikema Hommes, N. J. R. Dissected Nucleus-Independent Chemical Shift Analysis of π-Aromaticity and Anti-aromaticity. *Org. Lett.* **2001**, *3*, 2465–2468.
- (84) Chen, Z.; Wannere, C. S.; Corminboeuf, C.; Puchta, R.; Schleyer, P. V. R. Nucleus-Independent Chemical Shifts (NICS) as an Aromaticity Criterion. *Chem. Rev.* **2005**, *105*, 3842–3888.
- (85) Vetere, V.; Adamo, C.; Maldivi, P. Performance of the ‘parameter free’ PBE0 functional for the modeling of molecular properties of heavy metals. *Chem. Phys. Lett.* **2000**, *325*, 99–105.
- (86) Panayiotidou, L.; Stylianou, M.; Arabatzis, N.; Drouza, C.; Lianos, P.; Stathatos, E.; Keramidas, A. D. Synthesis, crystal structure and luminescence of novel Eu³⁺, Sm³⁺ and Gd³⁺ complexes of 1,3,5- and 1,2,4-triazines. *Polyhedron* **2013**, *52*, 856–865.
- (87) Álvarez-Moreno, M.; de Graaf, C.; López, N.; Maseras, F.; Poblet, J. M.; Bo, C. Managing the Computational Chemistry Big Data Problem: The ioChem-BD Platform. *J. Chem. Inf. Model.* **2015**, *55*, 95–103.

□ Recommended by ACS

Building a ship: A Rare-Earth Metal–Organic Framework and Its Application in a Catalytic Photooxidation Reaction

Victor Quezada-Novoa, Ashlee J. Howarth, *et al.*

MAY 27, 2021

CHEMISTRY OF MATERIALS

READ ▾

Construction of Water-Stable Rare-Earth Organic Frameworks with Ambient High Proton Conductivity Based on Zirconium Sandwiched Heteropolytungstate

Yan-Hua Fan, Dong-Bin Dang, *et al.*

AUGUST 23, 2022

INORGANIC CHEMISTRY

READ ▾

Single-Crystal Synthesis and Diverse Topologies of Hexanuclear Ce^{IV}-Based Metal–Organic Frameworks

Yu-Feng Zhang, Junfeng Bai, *et al.*

AUGUST 06, 2020

INORGANIC CHEMISTRY

READ ▾

Mechanochemical Synthesis of Phosphonate-Based Proton Conducting Metal–Organic Frameworks

Max Rautenberg, Franziska Emmerling, *et al.*

JULY 01, 2022

INORGANIC CHEMISTRY

READ ▾

Get More Suggestions >